Global Biogeochemical Cycles

RESEARCH ARTICLE
10.1029/2023GB007788

Global Patterns of Surface Ocean Dissolved Organic Matter Stoichiometry

Zhou Liang[1], **Robert T. Letscher**[2], **and Angela N. Knapp**[1]

[1]Department of Earth, Ocean and Atmospheric Science, Florida State University, Tallahassee, FL, USA, [2]Earth Sciences | Ocean Process Analysis Laboratory, University of New Hampshire, Durham, NH, USA

Key Points:

- Surface ocean bulk and semi-labile dissolved organic matter (DOM) stoichiometry vary across ocean regions with global means of 387:26:1 and 179:20:1, respectively
- Surface ocean DOC:DOP and DON:DOP concentration ratios are more variable than DOC:DON concentration ratios
- Surface ocean gradients in P-depleted DOM stoichiometries in the Pacific and Atlantic basins reflect variable nutrient stress

Supporting Information:

Supporting Information may be found in the online version of this article.

Correspondence to:

Z. Liang,
zl18c@fsu.edu

Citation:

Liang, Z., Letscher, R. T., & Knapp, A. N. (2023). Global patterns of surface ocean dissolved organic matter stoichiometry. *Global Biogeochemical Cycles*, *37*, e2023GB007788. https://doi.org/10.1029/2023GB007788

Received 28 MAR 2023
Accepted 6 NOV 2023

Author Contributions:

Conceptualization: Zhou Liang, Robert T. Letscher, Angela N. Knapp
Data curation: Zhou Liang
Formal analysis: Zhou Liang
Funding acquisition: Robert T. Letscher, Angela N. Knapp
Investigation: Zhou Liang
Methodology: Zhou Liang, Robert T. Letscher, Angela N. Knapp
Project Administration: Robert T. Letscher, Angela N. Knapp
Resources: Zhou Liang, Robert T. Letscher, Angela N. Knapp

Abstract Surface ocean marine dissolved organic matter (DOM) serves as an important reservoir of carbon (C), nitrogen (N), and phosphorus (P) in the global ocean, and is produced and consumed by both autotrophic and heterotrophic communities. While prior work has described distributions of dissolved organic carbon (DOC) and nitrogen (DON) concentrations, our understanding of DOC:DON:DOP stoichiometry in the global surface ocean has been limited by the availability of DOP concentration measurements. Here, we estimate mean surface ocean bulk and semi-labile DOC:DON:DOP stoichiometry in biogeochemically and geographically defined regions using newly available marine DOM concentration databases. Global mean surface ocean bulk (C:N:P = 387:26:1) and semi-labile (C:N:P = 179:20:1) DOM stoichiometries are higher than Redfield stoichiometry, with semi-labile DOM stoichiometry similar to that of global mean surface ocean particulate organic matter (C:N:P = 160:21:1) reported in a recent compilation. DOM stoichiometry varies across ocean basins, ranging from 251:17:1 to 638:43:1 for bulk and 83:15:1 to 414:49:1 for semi-labile DOM C:N:P, respectively. Surface ocean DOP concentration exhibits larger relative changes than DOC and DON, driving surface ocean gradients in DOC:DON:DOP stoichiometry. Inferred autotrophic consumption of DOP helps explain intra- and inter-basin patterns of marine DOM C:N:P stoichiometry, with regional patterns of water column denitrification and iron supply influencing the biogeochemical conditions favoring DOP use as an organic nutrient. Specifically, surface ocean marine DOM exhibits increasingly P-depleted stoichiometries from east to west in the Pacific and from south to north in the Atlantic, consistent with patterns of increasing P stress and alleviated iron stress.

Plain Language Summary Dissolved organic matter (DOM) in the ocean is an important reservoir of carbon, nitrogen, and phosphorus that is made and used by living organisms in the ocean to sustain their growth. Here, we look at the stoichiometric ratios of these three elements in DOM across different surface ocean regions and find large changes in the ratios of carbon, nitrogen, and phosphorus in the DOM. The levels of phosphorus change more than the levels of carbon and nitrogen in DOM, and we attribute this to the preferential use of phosphorus in DOM by living organisms. We also find basin-scale changes in DOM stoichiometry across the Pacific and Atlantic Oceans and link these changes to patterns of water column denitrification and atmospheric iron supply, respectively.

1. Introduction

The ocean plays a critical role in the global carbon cycle, holding about 50 times as much carbon as does the atmosphere, and sequesters atmospheric carbon through its solubility and biological pumps (DeVries, 2022; Hain et al., 2014). The marine biological pump starts in the euphotic zone whereby phytoplankton transform inorganic carbon into organic matter through photosynthesis ("marine primary production"), followed by vertical export of that organic matter to the deep ocean ("marine export production") (DeVries, 2022; Emerson, 2014; Hain et al., 2014). Decades of effort have sought to understand the patterns and estimate the rates of marine primary and export production (e.g., Behrenfeld & Falkowski, 1997; DeVries & Weber, 2017; Emerson, 2014; Westberry et al., 2008). However, considerable uncertainty in and discrepancy between estimates of marine primary productivity and export productivity still exist (Carr et al., 2006; Emerson, 2014; Siegel et al., 2023). In particular, the fields of biological and chemical oceanography are still working to describe the processes that support marine primary and export production in subtropical gyres where inorganic nutrients are scarce (Emerson, 2014).

A range of nutrient sources have been evaluated for their potential to support marine productivity in subtropical gyres where nitrate (NO_3^-) and phosphate (PO_4^{3-}) concentrations are often at or below detection limits, yet rates

Software: Zhou Liang
Validation: Zhou Liang
Visualization: Zhou Liang
Writing – original draft: Zhou Liang
Writing – review & editing: Zhou Liang, Robert T. Letscher, Angela N. Knapp

of export production are comparable to more nutrient-replete regions (Emerson, 2014; Gruber et al., 1998; Johnson et al., 2010; Keeling et al., 2004). Candidate sources include subsurface inorganic nutrients entrained by a range of physical mechanisms (Kadko & Johns, 2011; Mahadevan, 2016; Stanley et al., 2015) and/or by vertically migrating phytoplankton (Villareal et al., 1993; Wirtz et al., 2022), atmospheric deposition (Baker et al., 2003; Jickells & Moore, 2015; Knapp et al., 2010), biological di-nitrogen (N_2) fixation (Knapp, McCabe, et al., 2018; Knapp et al., 2016, 2021), and organic nutrients (Knapp, Casciotti, & Prokopenko, 2018; Letscher et al., 2016; Lomas et al., 2010; Torres-Valdés et al., 2009). While all of these mechanisms are thought to contribute to marine production under different conditions, here we focus on evaluating the role of organic nutrients. Phytoplankton may utilize dissolved organic nitrogen (DON) or dissolved organic phosphorus (DOP) either after heterotrophic degradation that releases inorganic nutrients that are then assimilated, or by the direct assimilation of DON and/or DOP. A wide range of marine phytoplankton species including cyanobacteria, coccolithophores, diatoms, and dinoflagellates utilize DON and DOP directly when the supply of inorganic nutrients is not sufficient to meet their demands (e.g., Berges & Mulholland, 2008; Bronk et al., 2007; Duhamel et al., 2021; Dyhrman et al., 2006; Kathuria & Martiny, 2011; Li et al., 2018; Orchard et al., 2010; X. Zhang et al., 2020). For example, phytoplankton have been shown to release extracellular alkaline phosphatase and C-P lyase metalloenzymes to exploit P in DOP molecules (Duhamel et al., 2021; Dyhrman et al., 2006), while for DON, phytoplankton may use leucine aminopeptidase to access N in peptides (Berges & Mulholland, 2008; Bronk et al., 2007; X. Zhang et al., 2020). While the significance of organic nutrients in supporting marine production is expected to vary spatially, modeling studies suggest that DOP uptake by phytoplankton sustains >50% of annual net community production in the North Pacific and North Atlantic subtropical gyres (Letscher et al., 2016, 2022; Reynolds et al., 2014; Torres-Valdés et al., 2009).

While heterotrophs in the euphotic zone may consume dissolved organic matter (DOM) as an energy and C source, DON and DOP face an additional and unique demand as an assimilative nutrient source by autotrophs. Together with their higher biovolumes, autotrophic consumption of DON and DOP as nutrient sources is expected to drive surface ocean DOM stoichiometry away from that of its source, autotrophic production, and its associated "Redfield Ratio" stoichiometry (C:N:P = 106:16:1) (Redfield, 1934). Thus, interpreting variability in surface ocean DOM stoichiometry may provide insight into conditions where the utilization of DON and/or DOP supports marine primary productivity. Early efforts to measure DOC, DON and DOP concentrations and their ratios along a meridional transect in the North Pacific Ocean showed that bulk surface ocean DOC:DON:DOP concentration ratios varied significantly from the equatorial to the subarctic region (Abell et al., 2000). Recent work shows that the bulk surface ocean DOC:DON:DOP ratio at Station ALOHA in the North Pacific Ocean is ∼350:24:1 (Foreman et al., 2019) and at the BATS station in the North Atlantic Ocean is ∼983:68:1 (Singh et al., 2015), both relatively depleted in N and P compared with "Redfield" stoichiometry. Numerous additional observations and inversions describing the variability in surface ocean organic matter stoichiometry have emerged in recent years, often attributing the patterns to the plasticity of phytoplankton experiencing nutrient stress (DeVries & Deutsch, 2014; Galbraith & Martiny, 2015; Inomura et al., 2022; Martiny et al., 2013; Teng et al., 2014). However, most of these studies have investigated either marine particulate or total organic matter. The examination of the patterns and causes of marine DOM stoichiometric variability has been limited by the lack of global DON and DOP data sets, even though DOM is an important component of the biological pump, accounting for ∼20–25% of export productivity (Carlson et al., 1994; Hansell et al., 2009; Hopkinson & Vallino, 2005; Letscher et al., 2015; Roshan & DeVries, 2017; Siegel et al., 2023).

Here, we take advantage of new global surface ocean DOM data sets (Hansell et al., 2021; Liang et al., 2022b) which permit evaluation of basin-scale trends in DOC, DON, and DOP distributions and associated stoichiometry. The goals of this article are to: (a) describe basin-scale trends in surface ocean DOM concentration and its C:N:P stoichiometry, and (b) evaluate mechanisms consistent with inter-basin surface ocean DOM stoichiometric variability.

2. Methods

2.1. DOC, DON, and DOP Concentration Data Sets

The DOC and DON concentration data used here are from a recent compilation of global ocean observations from 1994 to 2021 (Hansell et al., 2021). The DOP concentration data used here are from the DOPv2021 database, which contains DOP concentration observations from 1990 to 2020 (Liang et al., 2022b). Only DOC

concentration data marked with the "good" quality flag (WOCE bottle flag = 2) were used, and similar data screening processes were used for the DON and DOP concentration data. The remaining DOC, DON, and DOP concentration data were binned onto the OCIM2 model grid with 2° × 2° horizontal resolution and 24 vertical layers (DeVries & Holzer, 2019; John et al., 2020) for further analysis. The OCIM2 grid (2° × 2°) was chosen to facilitate comparison with other recent modeling efforts (e.g., DeVries & Weber, 2017; Letscher et al., 2022; Wang et al., 2019; Xu & Weber, 2021) and to compensate for sparse and unevenly spaced data (Figure S1 in Supporting Information S1). After gridding, there were 24,458 DOC concentration, 5,679 DON concentration, and 1,878 DOP concentration observations at 2° × 2° resolution with 24 vertical layers. We assume that the data field represents the annual mean state since the DOC, DON, and DOP concentration data sets do not permit evaluation of seasonal trends, which near Bermuda are often within 20% of the mean, with variability more pronounced for DOC than for DON or DOP (Hansell & Carlson, 2001; Knapp et al., 2005; Lomas et al., 2010).

2.2. Global Ocean Partitioning

To study variability in DOM stoichiometry across the surface ocean, we divided the global ocean into 10 biogeochemical or geographical regions. First, we partitioned the global ocean into 10 biogeochemical regions according to Teng et al., 2014; Letscher et al., 2022. The boundaries between regions correspond to the annual mean 0.3 μM surface ocean PO_4^{3-} concentration contour. The regions include the Atlantic Subarctic (AtlSub), the North Atlantic Subtropical Gyre (NASG), the Atlantic equatorial region (EqAtl), the South Atlantic Subtropical Gyre (SASG), the Pacific Subarctic (PacSub), the North Pacific Subtropical Gyre (NPSG), the Pacific equatorial region (EqPac), the South Pacific Subtropical Gyre (SPSG), the Indian Ocean (IND), and the Southern Ocean (SO). We also evaluated variability in DOM stoichiometry using geographical divisions, including the Eastern North Atlantic (ENATL, 0°–65°N and 45°W–10°E), the Eastern South Atlantic (ESATL, 0°–40°S and 20°W–20°E), the Western North Atlantic (WNATL, 0°–65°N and 45°W–100°W), the Western South Atlantic (WSATL, 0°–40°S and 20°W–60°W), the Eastern North Pacific (ENPAC, 0°–65°N and 70°E–160°E), the Eastern South Pacific (ESPAC, 0°–40°S and 70°E–160°E), the Western North Pacific (WNPAC, 0°–65°N and 100°W–160°E), the Western South Pacific (WSPAC, 0°–40°S and 100°W–160°E), the Indian Ocean (Indian, 40°S–25°N and 20°E–145°E), and the Southern Ocean (Southern, >40°S).

2.3. Calculation of Bulk and Semi-Labile Surface Ocean DOC:DON:DOP Concentration Ratios

In every biogeochemical or geographical region, we took the mean of all bulk surface ocean DOC, DON and DOP concentration values for all 2° × 2° "bins" in the upper 73 m, and then used those mean bulk surface ocean DOC, DON and DOP concentrations in each region to calculate the mean bulk DOC:DON:DOP concentration ratios in each region. The upper 73 m was chosen to reflect the surface ocean because the upper 73 m corresponds to the top two vertical layers in the OCIM2 grid, which are often used to represent the euphotic zone (DeVries & Holzer, 2019; John et al., 2020; Letscher et al., 2022; Wang et al., 2019). We also calculated the DOM fractions in excess of the deep ocean DOM, which we defined as semi-labile DOM. Note that the DOM fraction calculated using this approach should include both labile and semi-labile fractions and we define this fraction as semi-labile DOM because labile DOM cycles on ∼hourly to daily timescales and is thus less likely to accumulate (Carlson & Hansell, 2015; Hansell, 2013). We subtracted the mean deep ocean bulk DOC, DON, and DOP concentrations for each region from the mean surface ocean bulk DOC, DON, and DOP concentrations to estimate the mean surface ocean semi-labile DOC, DON, and DOP concentrations, and from those the mean surface ocean semi-labile DOC:DON:DOP concentration ratios were calculated for each region. We assumed that the deep ocean (i.e., >1,000 m) DON concentration was 1.8 μM (Letscher & Moore, 2015), and that 0.05 μM was the mean deep ocean (i.e., >1,000 m) DOP concentration, as reported in the DOPv2021 database (Liang et al., 2022b) and at Station ALOHA (Foreman et al., 2019). While different mechanisms have been proposed for why DOC persists in the deep ocean (Arrieta et al., 2015; Dittmar et al., 2021; Druffel et al., 1992; Follett et al., 2014; Zakem et al., 2021), it is known that deep ocean DOC concentrations decrease slightly along the global ocean conveyor belt with the highest DOC concentrations found in the deep North Atlantic and lowest DOC concentrations in the deep North Pacific (Hansell & Carlson, 1998b). Thus, we used different deep (i.e., >1,000 m) ocean DOC concentrations to calculate surface semi-labile DOC concentration (DOC fractions in excess of the deep ocean DOC) in each region. Concentrations of deep ocean (>1,000 m) DOC were estimated at 44.4 μM in the North Atlantic, 41.5 μM in the South Atlantic, 39.6 μM in the Pacific, 42.2 μM in the Indian Ocean, and 41.9 μM in

Table 1
Mean Bulk Surface (<73 m) Ocean DOC, DON and DOP Concentrations (±1 S.D.) in the 10 Biogeochemical Regions, Where n_DOC, n_DON and n_DOP Represent the Number of DOC, DON and DOP Concentration Observations in Each Region

	DOC (μM)	n_DOC	DON (μM)	n_DON	DOP (μM)	n_DOP
AtlSub	68.7 ± 15.4	313	5.3 ± 1.7	94	0.12 ± 0.04	11
NASG	70.2 ± 8.6	493	4.8 ± 0.9	244	0.11 ± 0.07	229
EqAtl	73.5 ± 21.6	46	5.3 ± 1.1	43	0.20 ± 0.07	26
SASG	67.5 ± 6.3	130	4.4 ± 0.7	126	0.15 ± 0.07	89
IND	70.2 ± 4.8	247	4.8 ± 0.8	241	0.25 ± 0.06	18
SO	52.4 ± 8.3	569	3.7 ± 0.8	349	0.18 ± 0.09	67
PacSub	61.5 ± 7.5	234	4.5 ± 1.5	186	0.21 ± 0.11	46
NPSG	68 ± 6.3	228	4.4 ± 0.4	151	0.19 ± 0.08	93
EqPac	67.7 ± 6.4	154	4.5 ± 0.8	81	0.27 ± 0.06	39
SPSG	67.7 ± 6.8	228	4.2 ± 0.5	171	0.19 ± 0.06	141
Global mean	65.8	2642	4.5	1,686	0.17	759

the Southern Ocean (Lønborg et al., 2018). A sensitivity test using a constant deep ocean DOC concentration of 35 μM, DON concentration of 1.8 μM, and DOP concentration of 0.05 μM did not meaningfully change the DOM stoichiometry trends between the different biogeochemical regions (Table S1 in Supporting Information S1). We did not include the Arctic Ocean in this study due to limited DOP concentration observations from that basin.

2.4. Relationships Between Bulk Surface Ocean DOC, DON and DOP Concentrations and Net Primary Productivity

We performed correlation analyses between gridded surface ocean bulk DOC, DON, and DOP concentrations and rates of net primary productivity (NPP) (mol C m^{-2} yr^{-1}) by applying a Type II regression model in MATLAB with the function "gmregress" (Trujillo-Ortiz & Hernandez-Walls, 2021) and the uncertainty was estimated by using the bootstrap approach. In order to test the robustness of the correlations between surface ocean bulk DOC, DON, and DOP concentrations and rates of NPP, we used climatological NPP fields from two algorithms: the Carbon-based Productivity Model (CbPM) (Westberry et al., 2008) and the Vertically Generalized Productivity Model (VGPM) (Behrenfeld & Falkowski, 1997), both estimated from SeaWiFS chlorophyll *a* observations. We did not include samples from the Arctic Ocean in this correlation analysis because it is known that DOC concentrations in the Arctic are significantly influenced by river discharge, an external source of DOC to the ocean (Anderson & Amon, 2015) and because of limited DOP concentration observations from this basin.

3. Results

3.1. Global Patterns in Bulk Surface Ocean DOC, DON, and DOP Concentration Distributions

Concentrations of DOC in the surface ocean reflect the balance of their sources and sinks. The primary source of DOC in the ocean is marine photosynthesis (Carlson & Hansell, 2015) with secondary coastal inputs that are especially pronounced in the Arctic (Anderson & Amon, 2015; Benner et al., 2005; Hansell et al., 2004) and other areas of significant riverine (Gledhill et al., 2022; Medeiros et al., 2015; Raymond & Spencer, 2015) and/or submarine groundwater discharge (Connolly et al., 2020). Marine DOC is lost due to heterotrophic consumption (Carlson & Hansell, 2015; Hansell & Carlson, 1998b), which results in progressive decreases in DOC concentration with depth and along circulation pathways (Hansell & Carlson, 1998b). Additionally, DOC can be lost due to photolysis (Mopper et al., 2015) or hydrothermal circulation (Lang et al., 2006). Our calculations of mean surface ocean DOC concentrations for each region based on the recent compilation of global DOC concentration data (Hansell et al., 2021) reflect the impact of these inputs, with relatively high concentrations, ~68 μM, in tropical and subtropical surface waters (40°S–40°N), and relatively low concentrations in Southern Ocean surface waters, ~50 μM (Tables 1 and 2), consistent with previous observations and model output (Hansell et al., 2009;

Table 2
Mean Bulk Surface (<73 m) Ocean DOC, DON and DOP Concentrations (±1 S.D.) in the 10 Geographical Regions, Where n_DOC, n_DON and n_DOP Represent the Number of DOC, DON and DOP Concentration Observations in Each Region

Region	DOC (μM)	n_DOC	DON (μM)	n_DON	DOP (μM)	n_DOP
ENATL	67.0 ± 10.2	586	5.1 ± 1.3	206	0.13 ± 0.07	162
WNATL	75.5 ± 11.9	240	4.8 ± 0.8	150	0.10 ± 0.06	94
WSATL	70.1 ± 11.4	89	4.6 ± 0.9	85	0.15 ± 0.07	71
ESATL	66.0 ± 6.2	85	4.6 ± 0.7	74	0.16 ± 0.07	39
Indian	69.3 ± 5.5	275	4.8 ± 0.7	261	0.25 ± 0.06	21
Southern	50.4 ± 7.2	505	3.6 ± 0.9	304	0.14 ± 0.08	32
ENPAC	65.4 ± 7.0	236	4.5 ± 1.2	210	0.24 ± 0.10	62
WNPAC	66.0 ± 7.8	286	4.3 ± 0.8	145	0.17 ± 0.07	83
WSPAC	69.2 ± 8.7	104	4.3 ± 0.4	55	0.16 ± 0.04	62
ESPAC	66.2 ± 5.3	236	4.3 ± 0.6	196	0.22 ± 0.07	133
Global mean	65.8	2642	4.5	1,686	0.17	759

Roshan & DeVries, 2017). We also note that the standard deviations of mean surface ocean DOC concentrations in the EqAtl are high (73.5 ± 21.6 μM), potentially resulting from the seasonally variable input of DOC from the Amazon River (Gledhill et al., 2022; Raymond & Spencer, 2015).

While marine DON and DOP have the same sources as DOC, and they share the same sinks as DOC listed above, they can also be consumed by autotrophs as assimilative sources of N and P. Indeed, autotrophic consumption of DON and DOP in the surface ocean appears to be significant in the subtropical gyres when inorganic forms of N and P are scarce (Letscher et al., 2013, 2022; Mather et al., 2008). Regardless, variations in mean surface ocean DON concentration among regions are modest, with concentrations typically between 4.2 and 5.3 μM (Tables 1 and 2), also consistent with previous observations (Bif et al., 2022; Knapp, Casciotti, & Prokopenko, 2018; Knapp et al., 2011; Letscher et al., 2013). Mean regional surface ocean DON concentrations in the EqAtl and EqPac were 5.3 ± 1.1 μM and 4.5 ± 0.8 μM, respectively. In the NPSG, mean surface ocean DON concentrations were 4.4 ± 0.4 μM and in the SPSG were 4.2 ± 0.5 μM (Table 1). The lowest mean surface ocean DON concentrations were found in the SO, 3.7 ± 0.8 μM (Tables 1 and 2).

In contrast, mean bulk surface ocean DOP concentrations showed more variability than DOC or DON, with higher mean concentrations associated with regions of elevated upwelling and new production. For example, mean surface ocean DOP concentrations in the EqPac were 0.27 ± 0.06 μM, and in the EqAtl were 0.20 ± 0.07 μM, and were lower in subtropical gyres, 0.11 ± 0.07 μM in the NASG and 0.15 ± 0.07 μM in the SASG (Table 1), consistent with previous observations (Björkman & Karl, 2003; Hashihama et al., 2020; Liang et al., 2022b; Lomas et al., 2010; Mather et al., 2008). We note that the calculation of mean surface ocean DOP concentrations in the AtlSub and IND were based on small data sets ($n = 11$ for AtlSub and $n = 18$ for IND) due to limited observations from these two regions (Table 1). Additionally, DOP concentration measurements in the AtlSub from the DOPv2021 database were collected at sites adjacent to the NASG (Liang et al., 2022a), leading to potential bias. Further sampling for the Atlantic subpolar region and Indian Ocean is required.

3.2. Variations in Bulk Surface Ocean DOM Stoichiometry in Different Biogeochemical Regions

Bulk surface (<73 m) ocean DOC:DON:DOP concentration ratios varied among biogeochemical regions (Figures 1a–1c) (Table 3). DOC:DON concentration ratios in the different regions fell into a relatively narrow range, increasing by ~25% from 13.0:1 to 16.1:1, higher than the canonical Redfield ratio (C:N = 6.6:1), with relatively high DOC:DON concentration ratios found in the subtropical gyres, similar to previously reported bulk DOC:DON concentration ratios (Bif et al., 2022; Hansell & Carlson, 2001; Hopkinson & Vallino, 2005; Letscher & Moore, 2015). Bulk surface ocean DOC:DON concentration ratios in the NPSG, SPSG, NASG, and SASG fell within a narrower range and were 15.5:1, 16.1:1, 14.6:1, and 15.3:1, respectively (Figure 1a) (Table 3). Bulk DOC:DON concentration ratios in equatorial and subpolar regions were slightly lower, 15.0:1 in the EqPac, 13.7:1 in the PacSub, 13.9:1 in the EqAtl, 13.0:1 in the AtlSub, and 14.2:1 in the SO (Figure 1a) (Table 3).

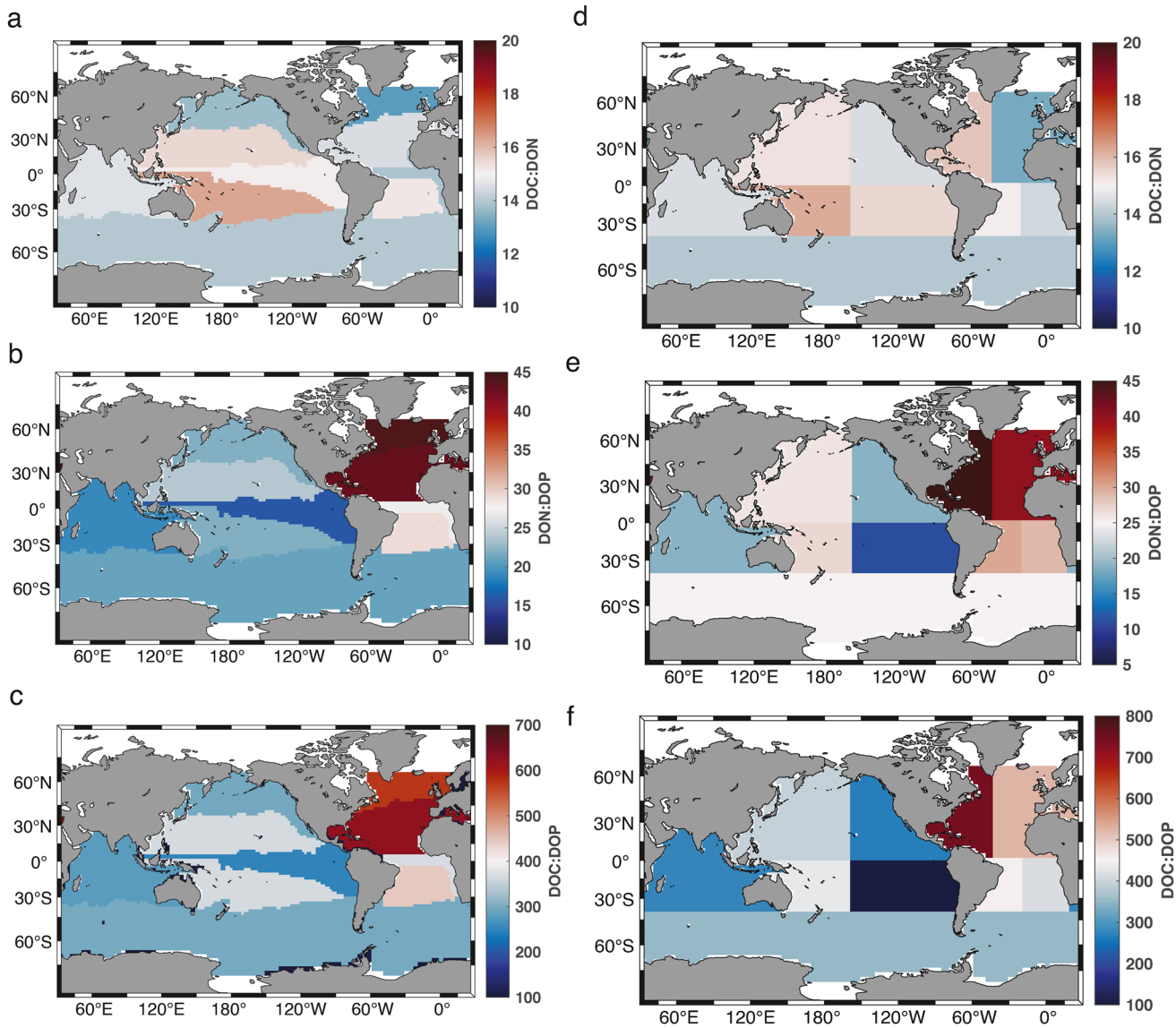

Figure 1. Surface (<73 m) ocean bulk DOC:DON (a), DON:DOP (b), and DOC:DOP (c) concentration ratios in different biogeochemical regions, and surface bulk DOC:DON (d), DON:DOP (e), and DOC:DOP (f) concentration ratios in different geographical regions.

In contrast, bulk surface ocean DON:DOP concentration ratios were more variable than bulk surface ocean DOC:-DON concentration ratios and exhibited a 2.5-fold increase from 17:1 in the EqPac to 44:1 in the AtlSub (Figure 1b) (Table 3). Bulk surface ocean DON:DOP concentration ratios in the PacSub were 21:1, in the SPSG were 22:1, and in the NPSG were 23:1 (Figures 1b and 1c) (Table 3). The Atlantic Ocean generally had higher DON:DOP concentration ratios than the Pacific. For example, the bulk surface ocean DON:DOP concentration ratios in the EqAtl were 27:1, in the SASG were 29:1, in the NASG were 43:1, and were 44:1 in the AtlSub (Figure 1b) (Table 3). We note that the high bulk surface ocean DON:DOP concentration ratios in the AtlSub were potentially biased by the limited DOP concentration observations in the region (n = 11, Table 1), with most of the observations collected near the neighboring subtropical gyre (NASG) (Liang et al., 2022b), which has elevated bulk surface ocean DOC:DOP and DON:DOP concentration ratios. Finally, bulk surface ocean DON:DOP concentration ratios were 19:1 in the IND and 21:1 in the SO (Figure 1b) (Table 3), intermediate between the EqPac and EqAtl values, and we also note that the majority of the IND samples were collected near the SO (Liang et al., 2022b).

As was seen for bulk surface ocean DON:DOP concentration ratios, bulk surface ocean DOC:DOP concentration ratios were also more variable than DOC:DON concentration ratios and exhibited 2.5-fold increase from

Table 3
Mean (±1 S.D.) Bulk Surface (<73 m) Ocean DOC:DON, DON:DOP, and DOC:DOP Concentration Ratios in the 10 Biogeochemical Regions, Calculated From Table 1

Region	Mean DOC:DON	Mean DON:DOP	Mean DOC:DOP	Mean DOC:DON:DOP
AtlSub	13.0 ± 5.1	44 ± 20	573 ± 230	573:44:1
NASG	14.6 ± 3.3	43 ± 29	638 ± 414	638:43:1
EqAtl	13.9 ± 5.0	27 ± 11	368 ± 168	368:27:1
SASG	15.3 ± 2.8	29 ± 14	450 ± 214	450:29:1
IND	14.6 ± 2.6	19 ± 6	281 ± 70	281:19:1
SO	14.2 ± 3.8	21 ± 12	291 ± 153	291:21:1
PacSub	13.7 ± 4.9	21 ± 13	293 ± 158	293:21:1
NPSG	15.5 ± 2.0	23 ± 10	358 ± 154	358:23:1
EqPac	15.0 ± 3.0	17 ± 5	251 ± 61	251:17:1
SPSG	16.1 ± 2.5	22 ± 7	356 ± 118	356:22:1
Global mean	14.6	26	387	387:26:1

a low of 251:1 in the EqPac to a high of 638:1 in the NASG. Bulk surface ocean DOC:DOP concentration ratios in the PacSub were 293:1 and higher in the NPSG and SPSG, 358:1 and 356:1, respectively (Figure 1c) (Table 3). As was seen for DON:DOP, bulk surface ocean DOC:DOP concentration ratios in the Atlantic were higher than those in the Pacific. In the EqAtl the bulk DOC:DOP concentration ratios were 368:1, in the SASG were 450:1, in the AtlSub were 573:1, and in the NASG were 638:1 (Figure 1c) (Table 3). Finally, bulk surface ocean DOC:DOP concentration ratios were 281:1 and 291:1 in the IND and SO, respectively (Figure 1c) (Table 3).

In summary, bulk surface ocean DOM concentration ratios were depleted in N and P compared with the canonical Redfield ratio (C:N:P = 106:16:1), and ranged from 251:17:1 in the EqPac to 638:43:1 in NASG (Table 3), with a global mean of 387:26:1. Smaller regional variations in bulk DOC:DON concentration ratios were observed than in bulk DON:DOP and DOC:DOP concentration ratios, which were largely driven by changes in DOP concentration. Two patterns in bulk surface ocean DOM stoichiometry emerged (a) bulk DON:DOP and DOC:DOP concentration ratios were lower in the equatorial and subpolar regions than those in the subtropical gyres; and, (b) bulk surface ocean DON:DOP and DOC:DOP concentration ratios were higher in the Atlantic than in the Pacific (Figures 1b and 1c) (Table 3).

3.3. Variations in Bulk Surface Ocean DOM Stoichiometry in Different Geographical Regions

Variations in bulk surface ocean DOM stoichiometry were also evaluated among geographical divisions of ocean basins, which allowed us to compare stoichiometric differences between the Western and Eastern or Southern and Northern regions of the Atlantic and Pacific Oceans, which are not apparent from the biogeochemical divisions (Figures 1d–1f). In the Atlantic Ocean, bulk surface ocean DOC:DON concentration ratios showed no notable differences between Western and Eastern regions or Southern and Northern regions, which were 15.7:1 in the WNATL, 13.1:1 in the ENATL, 15.2:1 in the WSATL, and 14.3:1 in ESATL (Table 4). A similarly narrow range in bulk surface ocean DOC:DON concentration ratios were found in the Pacific Ocean, which ranged from 14.5:1 to 16.1:1 (Table 4). Bulk surface ocean DOC:DON concentration ratios in the WNPAC, ENPAC, WSPAC, and ESPAC were 15.3:1, 14.5:1, 16.1:1, and 15.4:1, respectively (Figures 1–3).

Table 4
Mean (±1 S.D.) Bulk Surface (<73 m) Ocean DOC:DON, DON:DOP, and DOC:DOP Concentration Ratios in the 10 Geographical Regions, Calculated From Table 2

Region	Mean DOC:DON	Mean DON:DOP	Mean DOC:DOP	Mean DOC:DON:DOP
ENATL	13.1 ± 3.9	39 ± 23	515 ± 288	515:39:1
WNATL	15.7 ± 3.6	48 ± 30	755 ± 468	755:48:1
WSATL	15.2 ± 3.9	31 ± 16	467 ± 231	467:31:1
ESATL	14.3 ± 2.6	29 ± 13	413 ± 185	413:29:1
Indian	14.4 ± 2.4	19 ± 5	277 ± 70	277:19:1
Southern	14.0 ± 4.0	26 ± 16	360 ± 212	360:26:1
ENPAC	14.5 ± 4.2	19 ± 9	273 ± 117	273:19:1
WNPAC	15.3 ± 3.4	25 ± 11	388 ± 166	388:25:1
WSPAC	16.1 ± 2.5	27 ± 7	433 ± 121	433:27:1
ESPAC	15.4 ± 2.5	20 ± 7	301 ± 99	301:20:1
Global mean	14.6	26	387	387:26:1

Differences in bulk surface ocean DON:DOP concentration ratios in the Pacific were more pronounced between the East and West than between the North and South. In the ENPAC and ESPAC, bulk surface ocean DON:DOP concentration ratios were 19:1 and 20:1, but increased to 25:1 and 27:1 in the WNPAC and WSPAC, respectively (Figure 1e) (Table 4). In contrast, differences between bulk surface ocean DON:DOP concentration ratios were larger between the North and South Atlantic regions compared to the Eastern and Western regions (Figure 1e) (Table 4). Bulk surface ocean DON:DOP concentration ratios in the ESATL were 29:1 and in the WSATL were 31:1, while in the ENATL they were 39:1 and in the WNATL were 48:1 (Figure 1e) (Table 4).

Similar to DON:DOP, bulk surface ocean DOC:DOP concentration ratios had greater differences between the Western and Eastern regions than between the Northern and Southern regions of the Pacific. The bulk surface ocean DOC:DOP concentration ratios were 273:1 and 301:1 in the ENPAC and ESPAC, respectively, while in the WNPAC, they were 388:1 and in the WSPAC were 433:1 (Figure 1f) (Table 4). In contrast, differences in bulk surface ocean DOC:DOP concentration ratios were larger between the North and South than between the East and West in the Atlantic Ocean (Figure 1f) (Table 4). Bulk surface ocean DOC:DOP concentration ratios in the ESATL were 413:1 and in the WSATL were 467:1, while in the ENATL they were

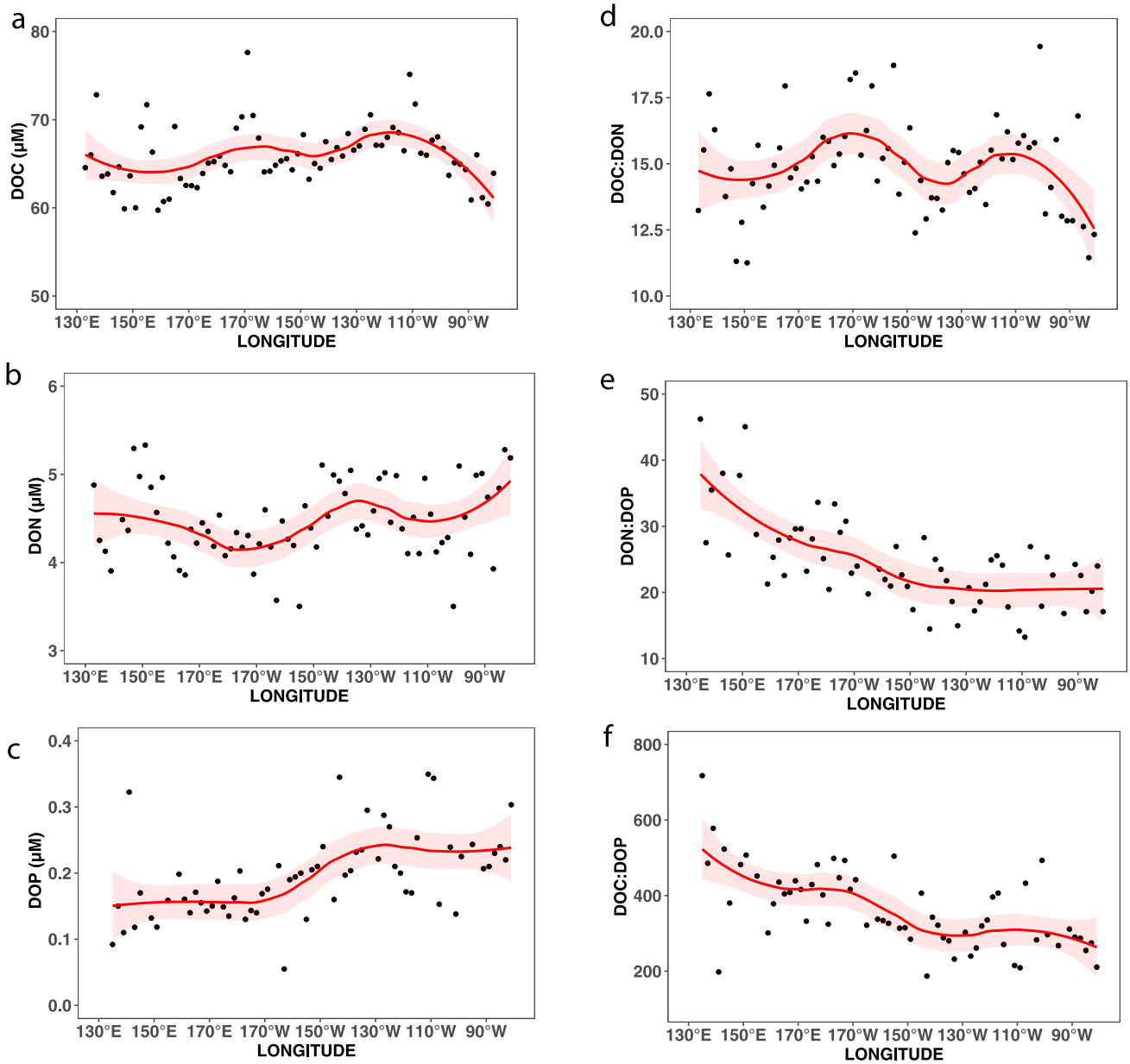

Figure 2. Combined North and South Pacific zonal mean surface (<73 m) ocean bulk DOC (a), DON (b), and DOP concentration (c), as well as bulk surface ocean DOC:DON (d), DON:DOP (e), and DOC:DOP (f) concentration ratios. The red line shows the fitting curve of the data using the LOWESS method (Cleveland, 1979) and the red shading area shows the 95% confidence interval.

515:1 and in the WNATL they were 755:1 (Figure 1f) (Table 4). The relatively high bulk DOC:DOP and DON:DOP concentration ratios found in the WNATL are consistent with the very low DOP concentrations previously observed in Sargasso Sea (Lomas et al., 2010; Mather et al., 2008).

To further identify potential large-scale gradients in bulk surface ocean DOM stoichiometry, we calculated zonal-mean, bulk surface ocean DOC:DON, DON:DOP, and DOC:DOP concentration ratios in the Pacific, and meridional-mean, bulk surface ocean DOC:DON, DON:DOP, and DOC:DOP concentration ratios in the Atlantic Oceans (Figures 2 and 3). In both cases, we used robust locally weighted regression (LOWESS) in R (Cleveland, 1979) to fit the points along the line of latitude or longitude to capture the zonal or meridional trends. Mean bulk surface ocean DOC:DON concentration ratios in the Pacific exhibited limited variability (~50%), ranging from ~12:1 to 18:1, but mean bulk surface ocean DON:DOP and DOC:DOP concentration ratios exhibited two-fold increases when comparing ratios West versus East of 160°W (Figure 2). In particular, mean bulk

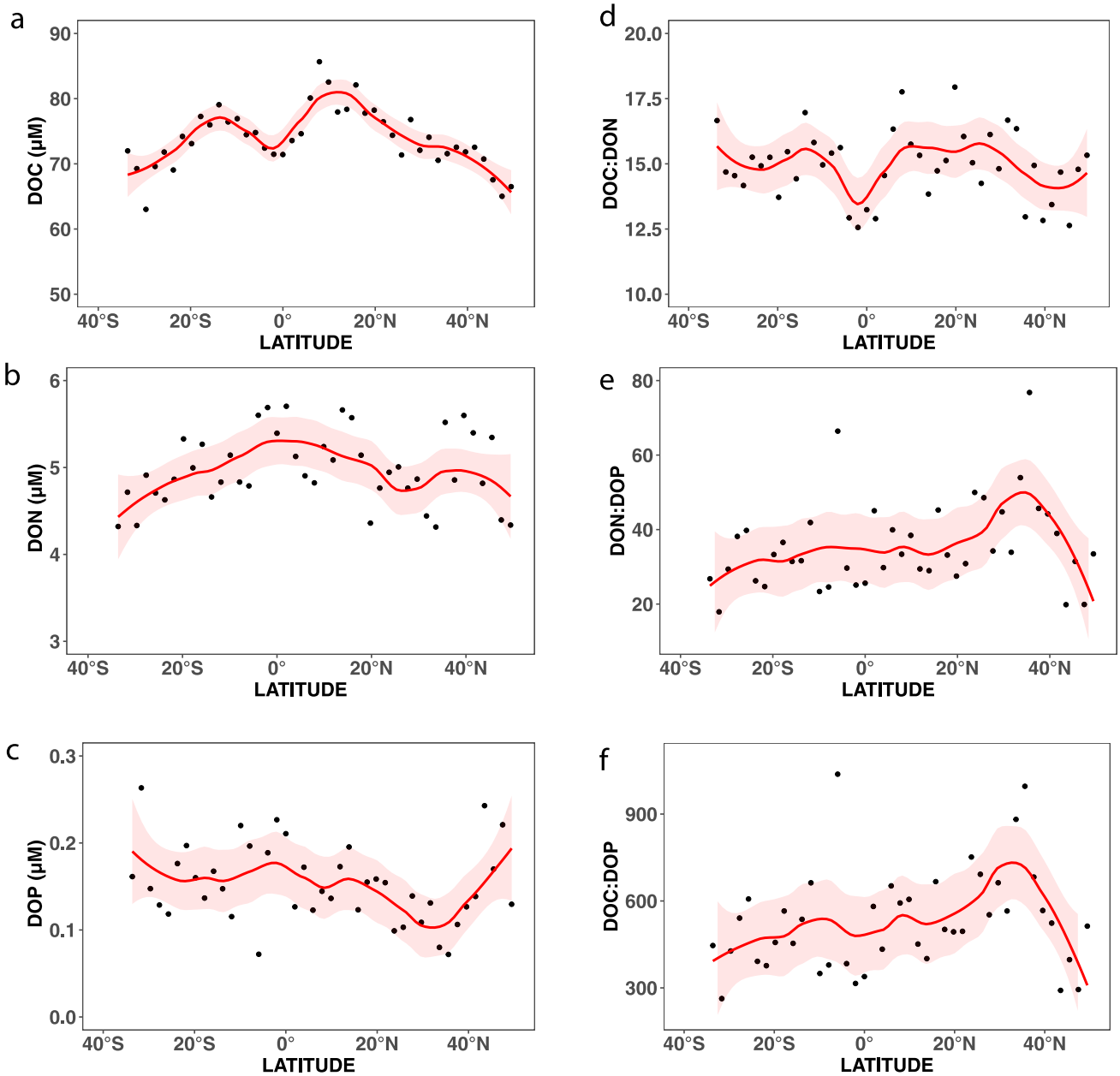

Figure 3. Combined West and East Atlantic mean meridional bulk surface ocean (<73 m) DOC (a), DON (b), and DOP (c) concentrations as well as bulk surface ocean DOC:DON (d), DON:DOP (e), and DOC:DOP (f) concentration ratios. The red line shows the fitting curve of the data using the LOWESS method (Cleveland, 1979) and the red shading area shows the 95% confidence interval.

surface ocean DON:DOP concentration ratios increased from ~20:1 to ~40:1 from east to west of 160°W and mean bulk surface ocean DOC:DOP concentration ratios increased from ~250:1 to ~500:1 from east to west of 160°W (Figure 2). In the Atlantic Ocean, the most pronounced DOM stoichiometric gradient occurred meridionally. While bulk surface ocean DOC:DON concentration ratios in the Atlantic Ocean were relatively invariant around ~15:1, bulk surface ocean DON:DOP and DOC:DOP concentration ratios exhibited two fold increases from South to North, reaching maxima of ~45:1 and ~700:1, respectively, between 20°N and 40°N compared to ratios observed between 30°S to 20°S, ~25:1 and 350:1, respectively (Figure 3). The majority of these increases in DON:DOP and DOC:DOP concentration ratios were driven by decreasing DOP concentrations between the South and North Atlantic.

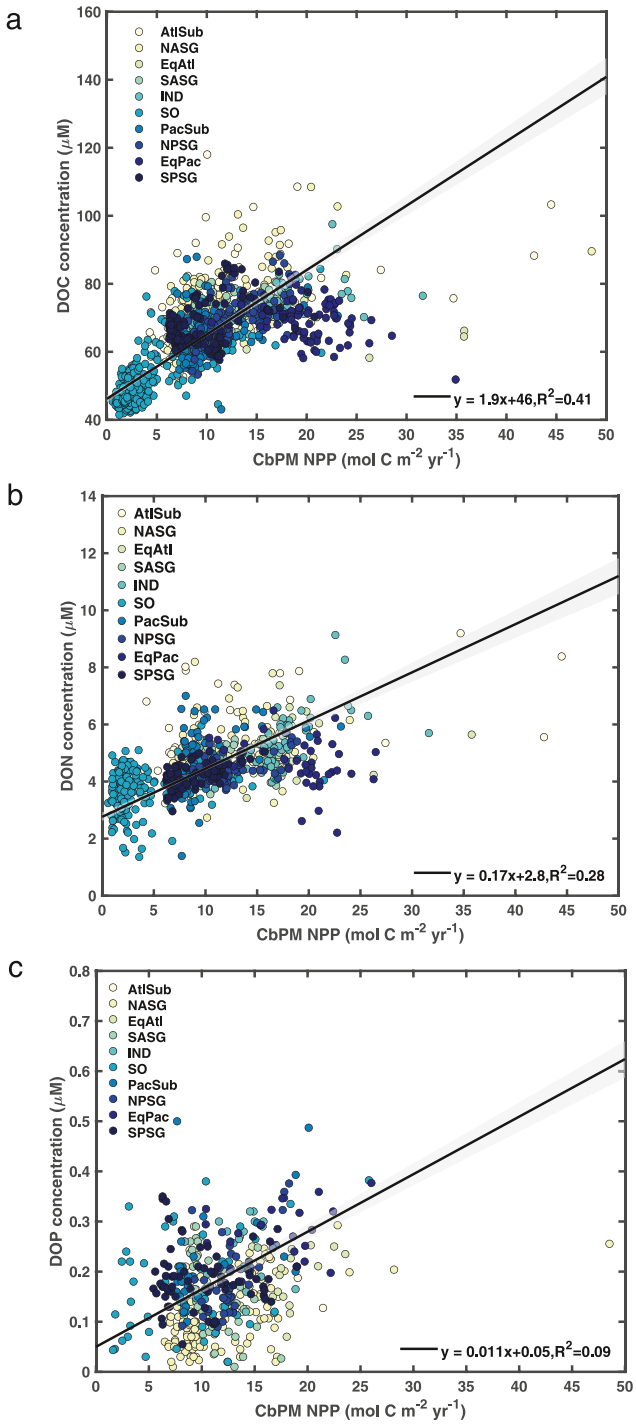

Figure 4. Type II linear regressions of bulk surface (<73 m) ocean DOC concentrations (a), DON concentrations (b), and DOP concentrations versus Net Primary Productivity determined by the Carbon-based Productivity Model (CbPM) (*y*-intercept fixed at 0.05) (Westberry et al., 2008). "AtlSub": Atlantic Subarctic region; "NASG": North Atlantic Subtropical Gyre; "EqAtl": Equatorial Atlantic region; "SASG": South Atlantic Subtropical Gyre; "IND": Indian Ocean; "SO": Southern Ocean; "PacSub": Pacific Subarctic region; "NPSG": North Pacific Subtropical Gyre; "EqPac": Equatorial Pacific region; "SPSG": South Pacific Subtropical Gyre. Gray shadings represent 95% confidence bands.

In summary, two patterns were identified from the geographical divisions that were not clear from the biogeochemical divisions: (a) bulk surface ocean DOC:DON:DOP concentration ratios increased from ~250:20:1 in the East to ~500:40:1 in the West in the Pacific Ocean, and, (b) bulk surface ocean DOC:DON:DOP concentration ratios increased meridionally from the South to the North in the Atlantic Ocean to maxima of ~700:45:1 between 20°N and 40° N.

3.4. Relationships Between Surface Ocean DOM Concentrations and Rates of NPP

To evaluate patterns in DOM production and consumption, we calculated correlations of bulk surface ocean DOC, DON, and DOP concentrations with satellite-derived rates of NPP using the Carbon-based Productivity Model (CbPM) (Westberry et al., 2008). Given that NPP is the primary source of DOM to the surface ocean (Carlson & Hansell, 2015), it is not surprising that bulk surface ocean DOC, DON, and DOP concentrations are all statistically significantly correlated with rates of NPP (Figure 4). Indeed, similar results have been previously observed for DOC (Hansell & Carlson, 1998a; Romera-Castillo et al., 2016), DON (Knapp, Casciotti, & Prokopenko, 2018; Letscher et al., 2013; R. Zhang et al., 2020), and DOP (Liang et al., 2022a). However, the correlation between bulk surface ocean DOC concentration and CbPM-derived rates of NPP is stronger than between CbPM-derived rates of NPP and surface ocean DON or DOP concentrations; DOC versus rates of NPP had a $R^2 = 0.41$ and $p < 0.0000001$, whereas for DON the R^2 was 0.28 and $p < 0.0000001$, and for DOP the R^2 was 0.09 and $p < 0.0000001$, respectively, evaluated using a Type II regression model (reduced major axis regressions) (Figure 4). The weaker correlation between CbPM-derived rates of NPP and surface ocean DON and DOP concentrations compared with DOC indicates that some quantitatively significant process is impacting surface ocean DON and DOP concentrations that is not impacting DOC concentrations, and we argue that the process is the assimilation of DON and DOP by autotrophs as nutrient sources. Importantly, the y-intercepts for the relationships between bulk surface ocean DOC and DON concentrations and CbPM-derived NPP rates were 46 μM and 2.8 μM, respectively, consistent with the concentration of deep ocean (>1,000 m) "refractory" DOC and DON calculated from the DOC and DON concentrations database (Hansell et al., 2021) (Table 5). However, the *y*-intercept for the relationship between bulk surface ocean DOP concentration and NPP rates derived from either VGPM or CbPM algorithm was a small negative number (−0.05 μM) (Table S2 in Supporting Information S1). We note that a number of surface ocean DOP concentration data from the North Atlantic fall below the best fit regression line, while data from the Eastern Pacific fall above the line, contributing to the negative intercept (Figure 4c). Low DOP concentrations were observed in the North Atlantic, consistent with previous observations of elevated rates of DOP consumption due to elevated PO_4^{3-} stress (Dyhrman et al., 2006; Liang et al., 2022a; Lomas et al., 2010; Martin et al., 2014; Sohm & Capone, 2010; Van Mooy et al., 2009), which contributes to the negative *y*-intercept. This is further confirmed by performing a regression analysis for data in the Pacific Ocean and the Atlantic Ocean separately, which showed that the *y*-intercept for DOP and NPP relationship is 0.02 μM in the Pacific Ocean but −0.05 in the Atlantic Ocean (Table S3 in Supporting Information S1). To capture the DOP production signal and the relationship between estimated rates of NPP and bulk surface ocean DOP concentrations, we aligned the *y*-intercept with the observations and set the *y*-intercept to 0.05 μM, which corresponds to the

Table 5
Semi-Labile and Refractory DOC:DON, DON:DOP, and DOC:DOP Concentration Ratios Determined Using Different NPP Data Products and Approaches

	DOC (μM)	DON (μM)	DOP (μM)	DOC:DON	DON:DOP	DOC:DOP	DOC:DON:DOP
Slope ratios (semi-labile DOM stoichiometry)							
CbPM NPP (DOP vs. NPP *y*-intercept fixed as 0.05)	-	-	-	11.2 ± 0.9	15.5 ± 1.0	173 ± 11	173:15.5:1
CbPM NPP (no fixed *y*-intercept)	-	-	-	11.2 ± 0.9	9.4 ± 1.2	106 ± 13	106:9.4:1
VGPM NPP (DOP vs. NPP *y*-intercept fixed as 0.05)	-	-	-	10.7 ± 0.8	16.6 ± 1.2	176 ± 12	176:16.6:1
VGPM NPP (no *y*-intercept fixed)	-	-	-	10.7 ± 0.8	12.1 ± 1.1	129 ± 12	129:12.1:1
CbPM NPP (Pacific Ocean data only)	-	-	-	11.3 ± 0.4	8.8 ± 0.8	100 ± 7	100:8.8:1
CbPM NPP (Atlantic Ocean data only)	-	-	-	10.6 ± 1.6	10.6 ± 1.3	119 ± 19	119:10.6:1
Mean				11.0 ± 0.9	12.2 ± 3.0	134 ± 30	134:12.2:1
y-intercept ratios (refractory DOM stoichiometry)							
CbPM NPP (DOP vs. NPP *y*-intercept fixed as 0.05)	46 ± 0.5	2.8 ± 0.1	0.05	16.5 ± 0.6	56 ± 2	920 ± 10	920:56:1
CbPM NPP (no fixed *y*-intercept)	46 ± 0.5	2.8 ± 0.1	−0.05 ± 0.02	16.5 ± 0.6	-	-	-
VGPM NPP (DOP vs. NPP *y*-intercept fixed as 0.05)	45 ± 0.8	2.5 ± 0.1	0.05	18.0 ± 0.8	50 ± 2	900 ± 16	900:50:1
VGPM NPP (no *y*-intercept fixed)	46 ± 0.4	2.5 ± 0.1	−0.02 ± 0.01	18.0 ± 0.8	-	-	-
CbPM NPP (Pacific Ocean data only)	46 ± 0.4	2.8 ± 0.1	0.02 ± 0.01	16.5 ± 0.6	140 ± 70	2300 ± 1,150	2300:140:1
CbPM NPP (Atlantic Ocean data only)	49 ± 1.7	2.7 ± 0.2	−0.05 ± 0.02	18.1 ± 1.5	-	-	-
Mean	46 ± 1.5	2.7 ± 0.1	-	17.0 ± 0.8	82 ± 41	1,373 ± 655	1373:82:1
Deep ocean concentration average (refractory DOM stoichiometry)							
>1,000 m	42 ± 5.0	3.0 ± 1.0	0.05 ± 0.04	14.0 ± 5.0	60 ± 52	842 ± 679	842:60:1

Note. Ratios of the y-intercepts are not calculated if the *y*-intercept is negative. Values of slopes and y-intercepts used to calculate ratios can be found in Tables S2 and S3 in Supporting Information S1.

deep ocean (>1,000 m) DOP concentration observed at Station ALOHA (Foreman et al., 2019) as well as that calculated from the DOPv2021 database (Liang et al., 2022b), and then refitted the linear regression (Figure 4c).

We summarized the slope and intercept ratios by using different NPP products and methods to perform regression analysis in Table 5. To account for the uncertainties from using different NPP products and ways to perform regression analysis, we averaged slope and intercept ratios from those different approaches to give a "best estimate" ratio. Here, we consider the stoichiometry of the y-intercepts to reflect the DOC:DON:DOP concentration ratios of "refractory," or deep-ocean DOM, where rates of NPP = 0. In contrast, the ratio of the slopes can be considered the DOC:DON:DOP concentration ratio of "semi-labile" surface ocean DOM, or the stoichiometry of the DOM in excess of the deep ocean DOM. Using the VGPM NPP product (Behrenfeld & Falkowski, 1997) did not meaningfully alter the strength of the correlation between DOC, DON, and DOP concentrations versus rates of NPP ($R^2 = 0.36$, $p < 0.0000001$ for DOC vs. NPP, $R^2 = 0.28$, $p < 0.0000001$ for DON vs. NPP, and $R^2 = 0.07$, $p < 0.0000001$ for DOP vs. NPP), or the semi-labile or refractory DOM C:N:P ratios calculated from this method (Table 5). Our semi-labile DOC:DON:DOP concentration ratios are consistent with those reported in Hopkinson & Vallino, 2005, 199:20:1. Hopkinson & Vallino, 2005 reported refractory DOC:DON:DOP ratios as 3511:202:1 by using samples mainly collected in the North Atlantic, where the highest global ocean bulk DON:DOP and DOC:DOP concentration ratios and lowest DOP concentrations are found (Figure 1). Carefully measured deep ocean DOC:DON:DOP concentration ratios via improved methods at Station ALOHA in the North Pacific are 760:45:1 (Foreman et al., 2019). Our "best estimate" refractory DOC:DON:DOP concentration ratios (1373:82:1) fall between those reported in Hopkinson & Vallino, 2005; Foreman et al., 2019, likely representing the global average ratios.

3.5. Variations in Semi-Labile Surface Ocean DOM Stoichiometry in Different Biogeochemical Regions

Correlations between surface ocean DOC, DON, and DOP concentrations and rates of NPP indicate that removing the deep ocean DOM from surface ocean stoichiometry could allow us to focus on variability associated with DOC:DON:DOP production and consumption patterns unique to biogeochemically and geograph-

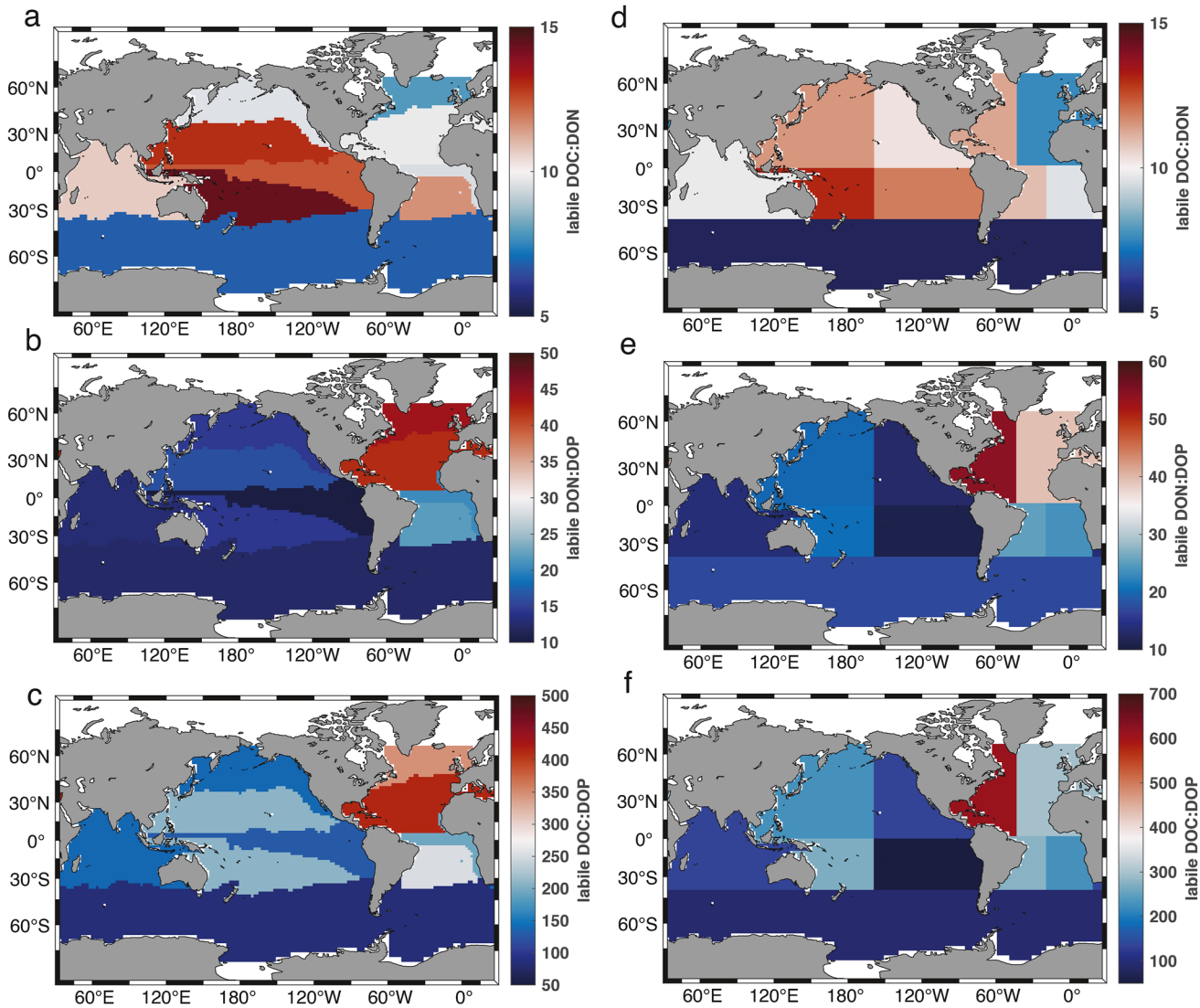

Figure 5. Semi-labile surface (<73 m) ocean DOC:DON (a), DON:DOP (b), and DOC:DOP (c) concentration ratios in different biogeochemical regions, and semi-labile surface ocean DOC:DON (d), DON:DOP (e), and DOC:DOP (f) concentration ratios in different geographical regions.

ically defined regions. We find that regional variations in semi-labile surface ocean DOM stoichiometry are similar to those observed for bulk surface ocean DOM stoichiometry, with generally lower ratios found in the equatorial and subpolar regions and higher concentration ratios found in the subtropical gyres (Figures 5a–5c) (Table 6). Additionally, semi-labile surface ocean DOM had higher DON:DOP and DOC:DOP concentration ratios but lower DOC:DON concentration ratios in the Atlantic Ocean than in the Pacific Ocean (Figures 5a–5c) (Table 6).

Broadly speaking, semi-labile surface ocean DOC:DON concentration ratios were lower, and thus closer to the "Redfield" C:N ratio of 6.6:1 than the bulk DOC:DON concentration ratios, and ranged from 5.4:1 to 12.0:1, or spanned a ∼100% range, a larger dynamic range than that observed for bulk surface ocean DOC:DON concentration ratios. Specifically, in the IND and SO, semi-labile surface ocean DOC:DON concentration ratios were 9.2:1 and 5.4:1, respectively (Figure 5a) (Table 6). In the EqPac and EqAtl, semi-labile surface ocean DOC:DON concentration ratios were 10.6:1 and 8.4:1, respectively, and in the PacSub and AtlSub were 8.1:1 and 7.0:1, respectively (Figure 5a) (Table 6). In the NPSG and SPSG, semi-labile surface ocean DOC:DON concentration ratios were 11.0:1 and 12.0:1, respectively, and in the NASG and SASG, they were 8.5:1 and 9.8:1, respectively (Figure 5a) (Table 6).

Table 6
Mean Semi-Labile (±1 S.D.) Surface (<73 m) Ocean DOC, DON and DOP Concentrations and Semi-Labile DOC:DON, DON:DOP, and DOC:DOP Concentration Ratios in the 10 Biogeochemical Regions

Region	slDOC (μM)	slDON (μM)	slDOP (μM)	slDOC:DON	slDON:DOP	slDOC:DOP	slDOC:DON:DOP
AtlSub	24.3 ± 16.3	3.5 ± 1.7	0.07 ± 0.06	7.0 ± 5.8	50 ± 51	346 ± 392	346:50:1
NASG	25.8 ± 10.0	3.0 ± 1.0	0.06 ± 0.08	8.5 ± 4.3	49 ± 63	414 ± 549	414:49:1
EqAtl	29.1 ± 22.2	3.5 ± 1.1	0.15 ± 0.08	8.4 ± 7.0	23 ± 14	195 ± 178	195:23:1
SASG	26.0 ± 8.2	2.6 ± 0.8	0.10 ± 0.08	9.8 ± 4.3	26 ± 21	254 ± 209	254:26:1
IND	27.8 ± 7.1	3.0 ± 0.9	0.20 ± 0.07	9.2 ± 3.6	15 ± 7	138 ± 58	138:15:1
SO	10.5 ± 9.8	1.9 ± 0.9	0.13 ± 0.09	5.4 ± 5.6	15 ± 13	83 ± 98	83:15:1
PacSub	22.0 ± 9.1	2.7 ± 1.5	0.16 ± 0.11	8.1 ± 5.8	17 ± 15	139 ± 114	139:17:1
NPSG	28.5 ± 8.2	2.6 ± 0.6	0.14 ± 0.09	11.0 ± 4.0	19 ± 12	209 ± 141	209:19:1
EqPac	28.2 ± 8.2	2.7 ± 0.9	0.22 ± 0.07	10.6 ± 4.7	12 ± 5	127 ± 53	127:12:1
SPSG	28.2 ± 8.6	2.4 ± 0.6	0.14 ± 0.07	12.0 ± 4.9	17 ± 9	209 ± 118	209:17:1
Global mean	25.0	2.8	0.14	8.9	20	179	179:20:1

As was seen for semi-labile surface ocean DOC:DON concentration ratios, semi-labile surface ocean DON:DOP concentration ratios were also lower than the bulk pool, ranging from 12:1 to 50:1, and thus were closer to the "Redfield" N:P ratio of 16:1. Generally, semi-labile surface ocean DON:DOP concentration ratios were lowest near regions of significant upwelling and/or new production and were higher in the subtropical gyres. For example, in the EqPac and EqAtl, semi-labile surface ocean DON:DOP concentration ratios were 12:1 and 23:1, respectively, and in the IND and SO were both 15:1 (Figure 5b) (Table 6). In the PacSub and AtlSub, semi-labile surface ocean DON:DOP concentration ratios diverged between the basins, and were 17:1 and 50:1, respectively. However, this Atlantic/Pacific difference needs further investigation due to limited DOP observations in the AtlSub (n = 11, Table 1). This Atlantic/Pacific difference is also observed in the subtropical gyres, with NPSG and SPSG semi-labile surface ocean DON:DOP concentration ratios of 19:1 and 17:1, respectively, while in the SASG and NASG, they were 26:1 and 49:1, respectively. We note that semi-labile surface ocean DON:DOP concentration ratios in the EqPac are lower than the canonical Redfield ratio, 12:1, which has not been reported before and is lower than the reported PON:POP ratios of ∼22:1 in the Pacific equatorial region (Lee et al., 2021).

Similar to DOC:DON and DON:DOP, the mean semi-labile surface ocean DOC:DOP concentration ratios observed in the biogeochemical regions were lower than the bulk surface ocean DOC:DOP concentration ratios, and ranged from 83:1 to 414:1 (Table 6), and thus were closer (and sometimes even lower than) the "Redfield" C:P ratio of 106:1. As was seen previously, lower mean semi-labile surface ocean DOC:DOP concentration ratios were observed in regions associated with upwelling and higher rates of NPP, and increased in the subtropical gyres. Specifically, in the EqPac and EqAtl, the mean semi-labile surface ocean DOC:DOP concentration ratios were relatively low, 127:1 and 195:1, respectively, similar to those in the IND and SO, 138:1 and 83:1, respectively (Figure 5c) (Table 6). Semi-labile surface ocean DOC:DOP concentration ratios increased in the subpolar gyres, 139:1 in the PacSub and 346:1 in the AtlSub (Figure 5c) (Table 6). In the NPSG and SPSG, semi-labile surface ocean DOC:DOP concentration ratios were both 209:1 and in the NASG and SASG they were 414:1 and 254:1, respectively (Figure 5c) (Table 6). In the SO, semi-labile surface ocean DOC:DOP and concentration ratios (C:P = 83:1) were also lower than the canonical Redfield ratio. However, lower-than Redfield POM C:P ratios have also been reported from the Southern Ocean in previous work (POM C:P = 91:1in Teng et al., 2014, and POM C:P = 61:1–190:1 in Lee et al., 2021).

In summary, semi-labile surface ocean DOC:DON:DOP concentration ratios ranged from 83:15:1 to 414:49:1 among biogeochemically divided regions, with a global mean of 179:20:1, and with typically lower stoichiometric ratios than in the bulk pool, with the low DOP concentrations observed in the NASG and AtlSub driving maxima in semi-labile DON:DOP and DOC:DOP concentration ratios (Figure 5) (Table 6).

Table 7
Mean (±1 S.D.) Semi-Labile Surface (<73 m) Ocean DOC, DON, and DOP Concentrations and Semi-Labile DOC:DON, DON:DOP, and DOC:DOP Concentration Ratios in the 10 Geographical Regions

	slDOC (μM)	slDON (μM)	slDOP (μM)	slDOC:DON	slDON:DOP	slDOC:DOP	slDOC:DON:DOP
ENATL	23.5 ± 11.8	3.3 ± 1.3	0.08 ± 0.09	7.1 ± 4.6	42 ± 51	299 ± 372	299:42:1
WNATL	31.3 ± 13.0	3.0 ± 0.9	0.05 ± 0.07	10.5 ± 5.3	58 ± 76	610 ± 813	610:58:1
WSATL	28.8 ± 12.6	2.8 ± 1.0	0.10 ± 0.08	10.1 ± 5.7	27 ± 22	276 ± 236	276:27:1
ESATL	24.6 ± 8.1	2.8 ± 0.8	0.11 ± 0.08	8.9 ± 3.9	26 ± 20	228 ± 185	228:26:1
Indian	27.1 ± 7.6	3.0 ± 0.9	0.20 ± 0.07	9.1 ± 3.6	15 ± 7	135 ± 61	135:15:1
Southern	8.6 ± 8.9	1.8 ± 0.9	0.09 ± 0.08	4.8 ± 5.6	19 ± 20	93 ± 126	93:19:1
ENPAC	26.0 ± 8.8	2.7 ± 1.2	0.19 ± 0.10	9.6 ± 5.4	14 ± 9	134 ± 83	134:14:1
WNPAC	26.6 ± 9.4	2.5 ± 0.9	0.12 ± 0.07	10.6 ± 5.2	22 ± 15	228 ± 166	228:22:1
WSPAC	29.8 ± 10.1	2.5 ± 0.6	0.11 ± 0.05	12.1 ± 5.0	22 ± 11	270 ± 153	270:22:1
ESPAC	26.9 ± 7.5	2.5 ± 0.8	0.17 ± 0.07	10.9 ± 4.5	14 ± 7	154 ± 78	154:14:1
Global mean	25.0	2.8	0.14	8.9	20	179	179:20:1

3.6. Variations in Surface Ocean Semi-Labile DOM Stoichiometry in Different Geographical Regions

Regional variations in semi-labile surface ocean DOM stoichiometry in the geographical regions are similar to those observed in the biogeochemical regions, with concentration ratios closer to the canonical Redfield ratio than the bulk DOM concentration ratios observed in the same regions (Figures 5d–5f) (Table 7). As was apparent in the bulk surface ocean DOM stoichiometry, the geographical divisions again highlight semi-labile DOM stoichiometric gradients between the Eastern and Western Pacific, and between the Eastern and Western Atlantic Oceans.

Surface ocean semi-labile DOC:DON concentration ratios in the geographical regions ranged from 4.8 to 12.1 and were generally lower near regions of elevated NPP, most notably in the Southern region where semi-labile surface ocean DOC:DON concentration ratios were 4.8:1 (Table 7). In the Pacific Ocean, we found no notable differences in semi-labile surface ocean DOC:DON concentration ratios between the Northern and Southern or Eastern and Western geographic regions. Surface ocean semi-labile DOC:DON concentration ratios in the ENPAC and ESPAC were 9.6:1 and 10.9:1, respectively, and in the WNPAC and WSPAC were 10.6:1 and 12.1:1, respectively (Table 7). In the Atlantic Ocean, differences in semi-labile surface ocean DOC:DON concentration ratios were also small. In the ENATL and ESATL, semi-labile surface ocean DOC:DON concentration ratios were 7.1:1 and 8.9:1, respectively and in the WNATL and WSATL, semi-labile surface ocean DOC:DON concentration ratios were 10.5:1 and 10.1:1, respectively.

Similar to bulk surface ocean DON:DOP concentration ratios, semi-labile surface ocean DON:DOP concentration ratios, which ranged from 14:1 to 58:1, were more variable than semi-labile surface ocean DOC:DON concentration ratios. However, semi-labile surface ocean DON:DOP concentration ratios were not meaningfully lower than bulk surface ocean DON:DOP ratios. Relatively low semi-labile surface ocean DON:DOP concentration ratios were observed in the Indian and SO, 14.8 and 19.3, respectively (Figure 5) (Table 7). In the Pacific Ocean, there were larger differences between semi-labile surface ocean DON:DOP concentration ratios in the East versus West than between the North versus South, similar to the bulk pool (Figure 5). Semi-labile surface ocean DON:DOP concentration ratios in the ENPAC and ESPAC were both 14:1 but increased to 22:1 in the WNPAC and WSPAC (Figure 5) (Table 7). In the Atlantic, the difference in semi-labile surface ocean DON:DOP concentration ratios was most pronounced between the North versus South. The ESATL and WSATL had semi-labile surface ocean DON:DOP concentration ratios of 26:1 and 27:1, while the ENATL and WNATL had semi-labile surface ocean DON:DOP concentration ratios of 42:1 and 58:1, respectively (Figure 5) (Table 7).

Similar patterns were observed for semi-labile surface ocean DOC:DOP concentration ratios, which ranged from 93:1 to 610:1, and were generally higher in the Western versus Eastern Pacific, and Northern versus Southern Atlantic. Again, the lowest semi-labile surface ocean DOC:DOP concentration ratios were found in the Southern and IND regions, 93:1 and 135:1, respectively. In the Pacific Ocean, semi-labile surface ocean DOC:DOP

concentration ratios in the ENPAC and ESPAC were 134:1 and 154:1, respectively, and increased to 228:1 and 270:1 in the WNPAC and WSPAC, respectively (Figure 5) (Table 7). In the Atlantic Ocean, the semi-labile surface ocean DOC:DOP concentration ratios in the ESATL and WSATL were 228:1 and 276:1, while in the ENATL and WNATL, they were 299:1 and 610:1, respectively (Figure 5) (Table 7).

In summary, the semi-labile surface ocean DOC:DON:DOP concentration ratios in the geographically defined regions ranged from 93:19:1 in the Southern to 610:58:1 in the WNATL (Table 7), and were typically closer to "Redfield" stoichiometry than the bulk surface ocean DOC:DON:DOP concentration ratios (268:19:1 to 745:47:1) (Table 4). Semi-labile surface ocean DON:DOP and DOC:DOP stoichiometry shared similar patterns to their bulk counterparts, and increased from East to West in the Pacific Ocean and from South to North in the Atlantic Ocean, with the highest semi-labile surface ocean DON:DOP and DOC:DOP stoichiometry found in the Sargasso Sea (20°N–40°N) of the WNATL.

4. Discussion

4.1. Variability in Bulk Surface Ocean DOM Stoichiometry Driven by Changes in Surface Ocean DOP Concentrations

Previous work has examined variability in bulk surface ocean DOC and DON concentrations as well as their concentration ratios, finding relatively small variations in DON concentrations and DOC:DON concentration ratios (Bif et al., 2022; Hansell & Carlson, 2001; Letscher et al., 2013; Sipler & Bronk, 2015). We similarly find relatively low variability in both bulk and semi-labile surface ocean DOC:DON concentration ratios (Figures 1 and 4) (Tables 1–6). Evaluating bulk global surface ocean DOC and DON concentration data together with new DOP concentration data (Liang et al., 2022b), we find that bulk and semi-labile surface ocean DON:DOP and DOC:DOP concentration ratios vary more than bulk and semi-labile surface ocean DOC:DON concentration ratios, indicating that variations in DON:DOP and DOC:DOP concentration ratios are driven by the relatively wide range in DOP concentrations compared to the ranges in surface ocean DOC and especially DON concentrations (Figures 1 and 4) (Tables 3–7). Indeed, according to the global ocean DOC, DON, and DOP concentration data sets (Hansell et al., 2021; Liang et al., 2022b), the typical range in bulk surface ocean DOC, DON, and DOP concentrations are 40–80 μM, 3–6 μM, and 0.05–0.6 μM, respectively. These concentration ranges correspond to a 100% increase between typical surface ocean DOC and DON minimum and maximum concentrations, but an 1,100% increase between the typical minimum and maximum surface ocean DOP concentrations. Thus, the order of magnitude larger variability in bulk surface ocean DOP concentrations relative to bulk surface ocean DOC and DON concentrations corresponds to the higher variability in surface ocean DON:DOP and DOC:DOP concentration ratios relative to bulk surface ocean DOC:DON concentration ratios.

We hypothesize that the high variability in bulk surface ocean DON:DOP and DOC:DOP concentration ratios is driven by changes in DOP concentrations due to DOP consumption by autotrophs. We note that while both autotrophs and heterotrophs consume/remineralize surface ocean DOP, the autotrophic consumption of DOP quantitatively dominates. For example, potential DOP utilization rates can be estimated by measuring alkaline phosphatase activity (APA) in the ocean. Mather et al., 2008 reported that mean surface ocean APA in June in the NASG was 2.44 $nMPh^{-1}/\mu gC$ and 0.84 $nMPh^{-1}/\mu gC$ in the SASG. These APA measurements were normalized to carbon biomass and included both phytoplankton (i.e., autotrophic) and bacterial (i.e., heterotrophic) biomass. We can estimate the relative contribution of phytoplankton and bacteria to APA by considering their carbon biomass separately. Here, we use the BATS site as an example, where APA, phytoplankton biomass and bacterial biomass are well-constrained. At the BATS site, the magnitude of bacterial abundance is $\sim 5 \times 10^8$ cells L^{-1} (Cavender-Bares et al., 2001). Assuming 12 fg C/bacterial cell ($1fg = 1 \times 10^{-5}$ g) (Simon & Azam, 1989), the carbon biomass of bacteria is 6 μg C L^{-1}. We estimate that the carbon biomass of phytoplankton from living phytoplankton represents 50% of the POC pool at the BATS site (Fawcett et al., 2011). The multi-year mean surface (<50 m) ocean POC concentration at the BATS site is 2.5 ± 1.2 μM (Martiny et al., 2014; Tanioka et al., 2022), with a corresponding carbon biomass of phytoplankton of ∼1.25 μM (15 μg C L^{-1}). Using the APA measurements of Mather et al. (2008) and biomass carbon estimates of phytoplankton and bacteria, phytoplankton represent ∼70% of APA and bacteria contribute to ∼30% of APA at the BATS site. We note that DOP remineralized by bacteria could also be taken up by phytoplankton and thus would not retain P in the standing stock of bacterial biomass P. This example shows that phytoplankton quantitatively dominate potential DOP utilization in the surface ocean due to their higher biomass.

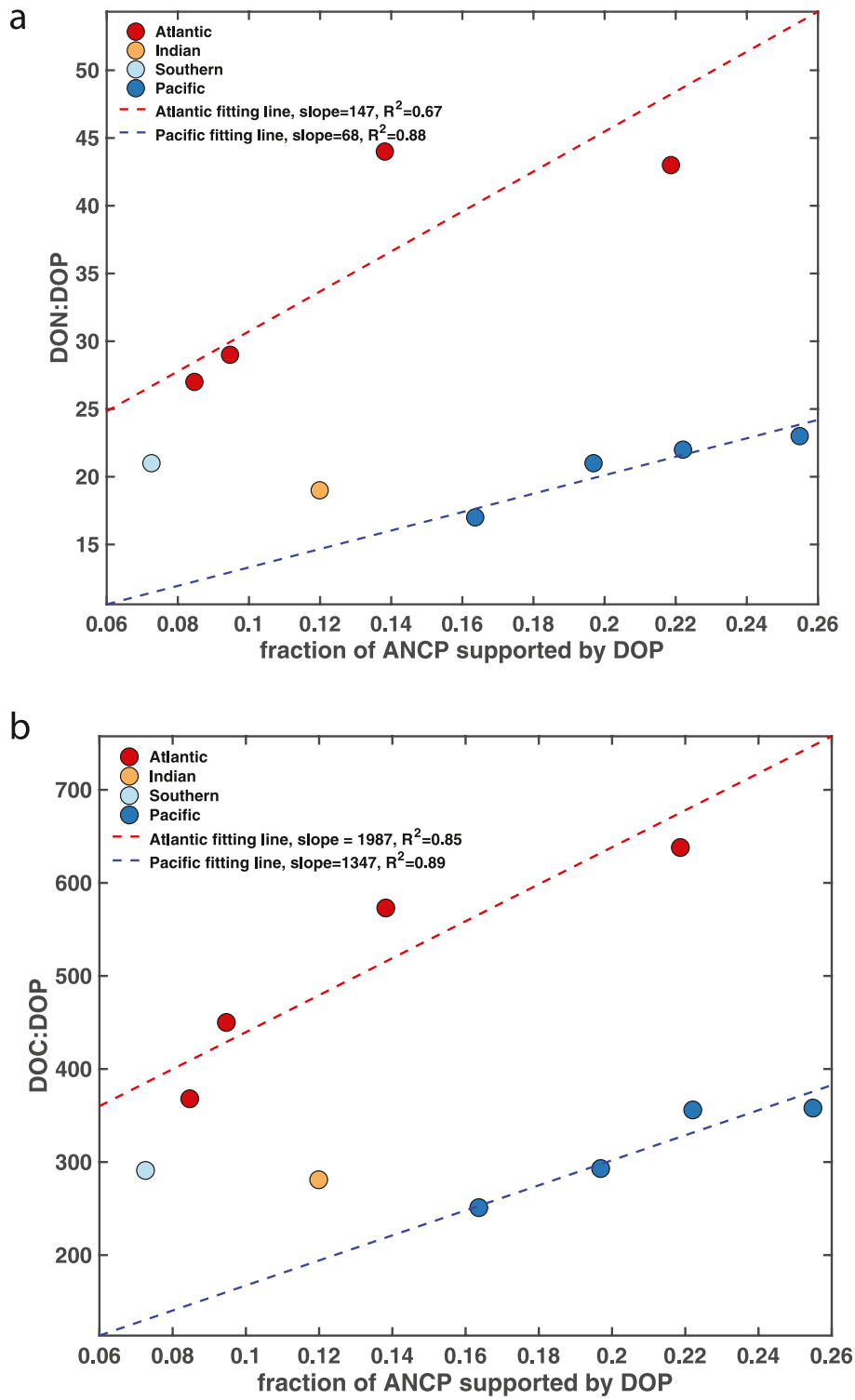

Figure 6. Correlations between bulk surface ocean DON:DOP (a) and DOC:DOP (b) concentration ratios versus the fraction of ANCP supported by DOP consumption. DON:DOP and DOC:DOP concentration ratios are from Table 3 and are based on biogeochemical divisions. Model-diagnosed fractions of ANCP supported by DOP consumption are from a data-constrained inverse model of the marine DOP cycle (Letscher et al., 2022).

To evaluate the relationship between variability in bulk surface ocean DON:DOP and DOC:DOP concentration ratios and DOP consumption by the autotrophic community in the surface ocean, we compared bulk surface ocean DON:DOP and DOC:DOP concentration ratios with a model product of the estimated fraction of annual net community production (ANCP) supported by DOP consumption, obtained from a data-constrained inverse model of the marine DOP cycle (Letscher et al., 2022) (Figure 6). Although no correlation for the global data set was found, we found positive correlations between bulk surface ocean DOC:DOP concentration ratios and the model-estimated fraction of ANCP supported by DOP consumption for points in the Pacific Ocean ($R^2 = 0.89$, slope = 1,347, $p < 0.05$) as well as separately for the Atlantic Ocean ($R^2 = 0.85$, slope = 1,987, $p < 0.05$) (Figure 6). Similarly, positive correlations between DON:DOP concentration ratios and the model-estimated fraction of ANCP supported by DOP consumption were also found for points in the Pacific Ocean ($R^2 = 0.88$, slope = 68, $p < 0.05$) and separately for the Atlantic Ocean ($R^2 = 0.67$, slope = 147, $p < 0.05$) (Figure 6). These positive correlations between bulk surface ocean DOC:DOP or DON:DOP concentration ratios and the fraction of ANCP supported by DOP consumption by surface ocean phytoplankton support the conclusion that DOP consumption by phytoplankton is the major contributor to changes in bulk surface ocean DOP concentrations, and the associated changes in bulk surface ocean DOC:DOP and DON:DOP concentration ratios. We interpret the higher bulk surface ocean DOC:DOP and DON:DOP concentration ratios and associated y-intercepts in Figure 6 for the Atlantic Ocean relative to the Pacific to imply that the Atlantic Ocean has a more P-depleted character relative to the Pacific Ocean, consistent with elevated rates of dissimilatory N loss in the Pacific versus Atlantic (see Section 4.2 below). Quantitatively, the slopes above suggest that for a 10% increase in the fraction of ANCP supported by DOP consumption in the Atlantic Ocean, DON:DOP and DOC:DOP concentration ratios increase by 15:1 and 135:1, respectively. In the Pacific Ocean, DON:DOP and DOC:DOP concentration ratios increase by 7:1 and 15:1, respectively, with a 10% increase in the fraction of ANCP supported by the DOP consumption. We suggest that these relatively large changes in surface ocean DOP concentrations due to autotrophic DOP consumption contribute to the zonal and meridional mean trends in bulk and semi-labile surface ocean DON:DOP and DOC:DOP concentration ratios observed in the Pacific Ocean and the Atlantic Ocean, respectively (Figures 3 and 4), which are explored further below.

4.2. Linkage Between Bulk and Semi-Labile Surface Ocean DOM Stoichiometry and Water Column Denitrification in the Pacific Ocean

The Pacific Ocean experiences greater West to East variability in bulk and semi-labile surface ocean DOM stoichiometry than between the North and South (Figure 1) (Tables 3 and 4). In particular, higher bulk surface ocean DOP concentrations are observed East versus West of ~160°W (Figure 2). These gradients in bulk surface ocean DOP concentration correspond to large gradients in bulk and semi-labile surface ocean DON:DOP and DOC:DOP stoichiometry zonally across the Pacific Ocean, with lower ratios in the Eastern versus Western Pacific Ocean (Figure 2). Previous work has suggested that zonal changes in DOP concentration across the Pacific can be attributed to the net production and accumulation of DOP in surface waters over oxygen deficient zones (ODZs), driven by dissimilatory NO_3^- consumption in suboxic subsurface waters (Liang et al., 2022a). The ODZs of both the Eastern Tropical North Pacific (ETNP) and Eastern Tropical South Pacific (ETSP) support significant rates of water column denitrification and/or anaerobic ammonium oxidation (Chang et al., 2010, 2012; DeVries et al., 2012; Ward et al., 2009) (Figure 2). The resulting "excess" supply of PO_4^{3-} compared to NO_3^- reduces demand on DOP and allows DOP to accumulate, and the accumulated DOP is then advected and consumed to the west (Liang et al., 2022a). At basin scales, this corresponds to zonal increases in bulk surface ocean DON:DOP and DOC:DOP concentration ratios from East to West (Figure 2).

In addition to direct measurements and modeled estimates of rates of water column denitrification and anammox, geochemical tracers such as "P*," where P* = ($[PO_4^{3-}]$–$[NO_3^-]$/16) (Deutsch et al., 2007), record the effects of water column denitrification and/or anaerobic ammonium oxidation. Here we compare modeled rates of water column denitrification (Wang et al., 2019) and zonally averaged surface ocean P* values calculated using World Ocean Atlas 2013 nutrient data (Garcia et al., 2013) with zonal trends in bulk surface ocean DON:DOP and DOC:DOP concentration ratios (Figure 7). Results show that Spearman's correlation coefficients for both zonal mean bulk surface ocean DON:DOP and DOC:DOP concentration ratios versus rates of water column denitrification are −0.58 ($p < 0.001$). Similarly, Spearman's correlation coefficients for both zonal mean bulk surface ocean DON:DOP and DOC:DOP concentration ratios versus P* are −0.55 ($p < 0.001$), indicating significant negative correlations between zonal trends of bulk surface ocean DON:DOP and DOC:DOP concentration ratios

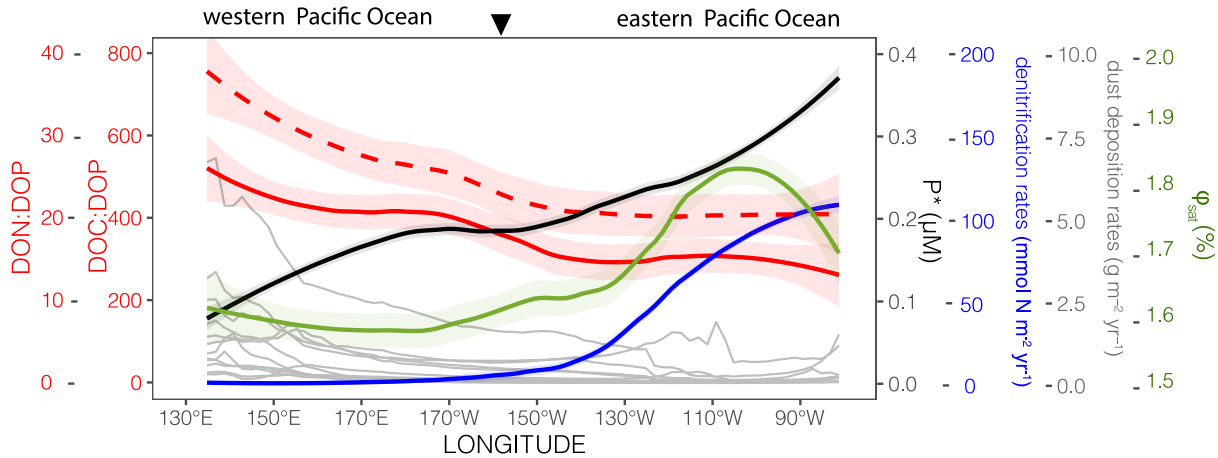

Figure 7. Combined North and South Pacific zonal mean bulk surface (<73 m) ocean DOC:DOP concentration ratios (solid red line, same data as in Figure 2), DON:DOP concentration ratios (dashed red line, same data as in Figure 2), surface ocean P* (black line), water column denitrification rates (Wang et al., 2019) (blue line), NPQ-corrected φ_{sat} (green line), and dust deposition rates from 12 different model outputs (Xu & Weber, 2021) (gray lines). Shadings reflect the 95% confidence interval. The black inverted triangle represents 160°W.

and rates of water column denitrification and P* in the Pacific Ocean (Figure 7). Similar results were found when comparing semi-labile surface ocean DOM stoichiometry with P* and modeled denitrification rates (Spearman's correlation coefficients = −0.56, $p < 0.001$ for semi-labile DON:DOP/DOC:DOP vs. rates of water column denitrification and Spearman's correlation coefficients = −0.53, $p < 0.001$ for semi-labile DON:DOP/DOC:DOP vs. P*).

The correlation between surface ocean DOM stoichiometry and water column denitrification rates is also apparent when comparing patterns of DOM stoichiometry in the Pacific Ocean with the Atlantic Ocean. The minimum oxygen concentration in the water column in the Eastern Atlantic is not low enough to enable denitrification (DeVries et al., 2012; Paulmier & Ruiz-Pino, 2009; Zehr & Ward, 2002), which results in a reduced supply of excess PO_4^{3-} to surface waters relative to the supply of NO_3^- and Redfieldian phytoplankton demands. Without significant rates of dissimilatory N loss in the water column of the Eastern Atlantic reducing demand on the surface ocean PO_4^{3-}, and thus DOP pools, we do not observe significant zonal gradients in bulk and semi-labile DON:DOP and DOC:DOP concentration ratios between the Eastern and Western Atlantic (Figure 1). Instead, we observe relatively higher bulk surface ocean DON:DOP concentration ratios in the Eastern Atlantic (~30:1–40:1) than in the Eastern Pacific, 19:1 (Table 4), with similar trends observed for bulk surface ocean DOC:DOP concentration ratios (Table 4). We interpret this to result from increased demand on the DOP pool in the Eastern Atlantic due to higher PO_4^{3-} stress. Consequently, we argue that water column denitrification in the ETNP and ETSP leaves a signature in bulk and semi-labile surface ocean DOM stoichiometry that effectively leads to a "subsidy" of DOP in Eastern Pacific surface waters compared to the Eastern Atlantic.

Although low surface ocean PO_4^{3-} concentrations and thus elevated PO_4^{3--} stress are the primary drivers of DOP consumption, recent work suggests that alleviated iron stress can enhance surface ocean DOP consumption (Liang et al., 2022a). In Figure 7, we overlay the zonal trends of 12 modeled dust deposition rates (Xu & Weber, 2021), as well as satellite-derived NPQ-corrected φ_{sat}, a remote-sensing-based estimate of iron stress experienced by phytoplankton (Behrenfeld et al., 2009; Liang et al., 2022a), to explore their relationships with surface ocean DOP distributions. Since modeled dust deposition patterns and rates are highly dependent on model choice, we consider the dust deposition output from 12 different atmospheric models (Xu & Weber, 2021). These 12 atmospheric models include 10 models from the AEROCOM Phase II Intercomparison project and two estimates from Mahowald et al., 2005; Zhang et al., 2015. NPQ-corrected φ_{sat} has been used to indicate iron stress experienced by marine phytoplankton (Behrenfeld et al., 2009; Browning et al., 2014; Hopwood et al., 2018; Lee et al., 2021; Liang et al., 2022a) based on phytoplankton photochemical and physiological relationships (Behrenfeld & Milligan, 2013), where higher NPQ-corrected φ_{sat} values correspond to elevated iron stress faced by phytoplankton. We find that modeled dust deposition rates increase and NPQ-corrected φ_{sat} decreases from East to West across the Pacific Ocean (Figure 7). Gradients in both metrics suggest that phytoplankton experience less iron stress in the Western than Eastern Pacific Ocean, consistent with observations that iron limits

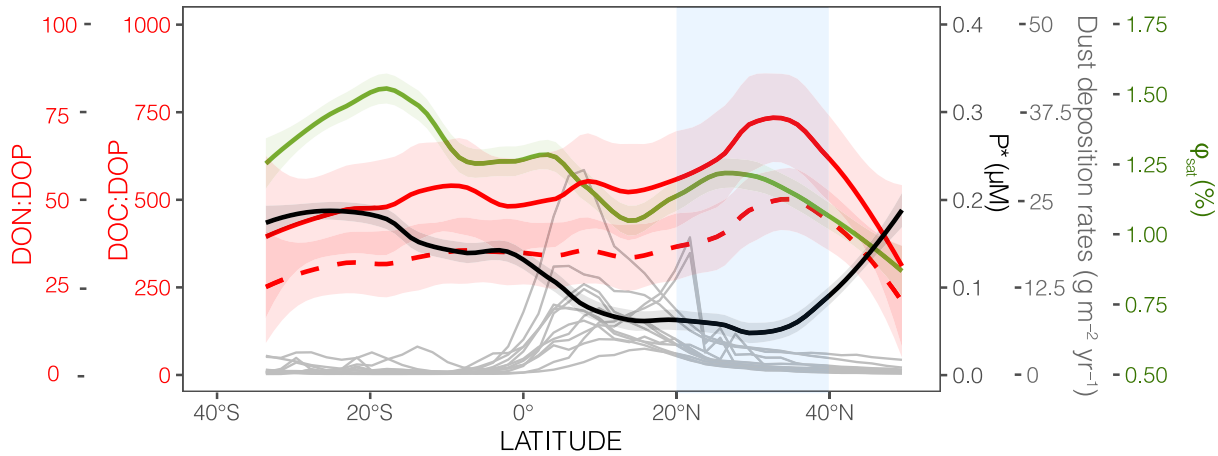

Figure 8. Combined Western and Eastern Atlantic meridional mean bulk surface (<73 m) ocean DOC:DOP concentration ratios (solid red line, same data as in Figure 3), DON:DOP concentration ratios (dashed red line, same data as in Figure 3), surface ocean P* calculated from World Ocean Atlas 2013 (Garcia et al., 2013) (black line), NPQ-corrected φ_{sat} (Behrenfeld et al., 2009) (green line), and dust deposition rates from 12 different model outputs (Xu & Weber, 2021) (gray lines). Blue shading marks the Sargasso Sea region (20°N–40°N). Red, green, and black shadings reflect the 95% confidence interval.

phytoplankton growth (Mahowald et al., 2005; Moore et al., 2013; Ustick et al., 2021) and nitrogen fixation rates (Dekaezemacker et al., 2013; Knapp et al., 2016) in the Eastern Pacific Ocean. We note that hydrothermal vents along the Tonga-Kermadec Ridge in the Western South Pacific Ocean are another potential source of iron in addition to dust deposition (Bonnet et al., 2023; Guieu et al., 2018). Increased iron supply in the Western South Pacific Ocean favors nitrogen fixation, which adds new nitrogen to the ocean and enhances PO_4^{3-} stress, highlighting DOP as an alternative P source to support primary production and nitrogen fixation. Thus, we interpret the increasing bulk and semi-labile surface ocean DON:DOP and DOC:DOP stoichiometry from East to West in the Pacific Ocean to result from progressive DOP consumption, in particular as PO_4^{3-} stress increases and iron stress decreases zonally.

4.3. Linkage Between Bulk and Semi-Labile DOM Stoichiometry and Iron Supply in the Atlantic Ocean

Here we explore potential causes of the meridional as opposed to zonal gradients in bulk and semi-labile surface ocean DOM stoichiometry observed in the Atlantic Ocean. In the Atlantic Ocean, the maximum bulk and semi-labile surface ocean DON:DOP and DOC:DOP concentration ratios were found in the Sargasso Sea (20°N–40°N) (Figures 3 and 8), coincident with the extraordinarily low DOP concentrations previously observed in this region, ~50 nM (Liang et al., 2022b; Lomas et al., 2010; Mather et al., 2008) (Figure 3). Indeed, the Sargasso Sea is the region where the highest bulk and semi-labile surface ocean DON:DOP and DOC:DOP stoichiometry is found not just in the Atlantic Ocean, but in the global ocean (Figures 1 and 2), highlighting the unique nature of this region. Previous work suggested that enhanced DOP consumption in this region occurs when phytoplankton face elevated PO_4^{3-} stress but iron stress is alleviated (Liang et al., 2022a). Similar to our analysis in the Pacific Ocean, we use meridionally-averaged, modeled dust deposition rates (Xu & Weber, 2021), NPQ-corrected φ_{sat} (Behrenfeld et al., 2009; Liang et al., 2022a), and surface ocean P* calculated from World Ocean Atlas 2013 (Garcia et al., 2013) to evaluate iron and PO_4^{3-} stress, respectively, in the Atlantic Ocean.

The minima in Atlantic surface ocean P* is found between 20°N and 40°N (Figure 8), indicative of elevated PO_4^{3-} stress in this region. The maxima of dust deposition rates estimated from the 12 models converged between 0° and 20°N, and NPQ-corrected φ_{sat} also decreases between 20°N and 40°N (Figure 8), suggesting reduced iron stress in this region. Reduced iron stress in the North Atlantic Ocean favors nitrogen fixation and thus enhances PO_4^{3-} stress (Wu et al., 2000), with DOP becoming a more important assimilative P source for phytoplankton. The maxima of DOC and DON concentrations in the Atlantic Ocean were also found between 0°N and 20°N, consistent with regional dust fertilization to phytoplankton (Figures 3 and 8). However, no notable increase in DOP concentrations is observed between 0° and 20°N, and the maxima in DON:DOP and DOC:DOP concentration ratios are found between 20°N and 40°N. We interpret these meridional trends to indicate that reduced iron stress from dust deposition enhances primary productivity to the extent that phytoplankton can access adequate

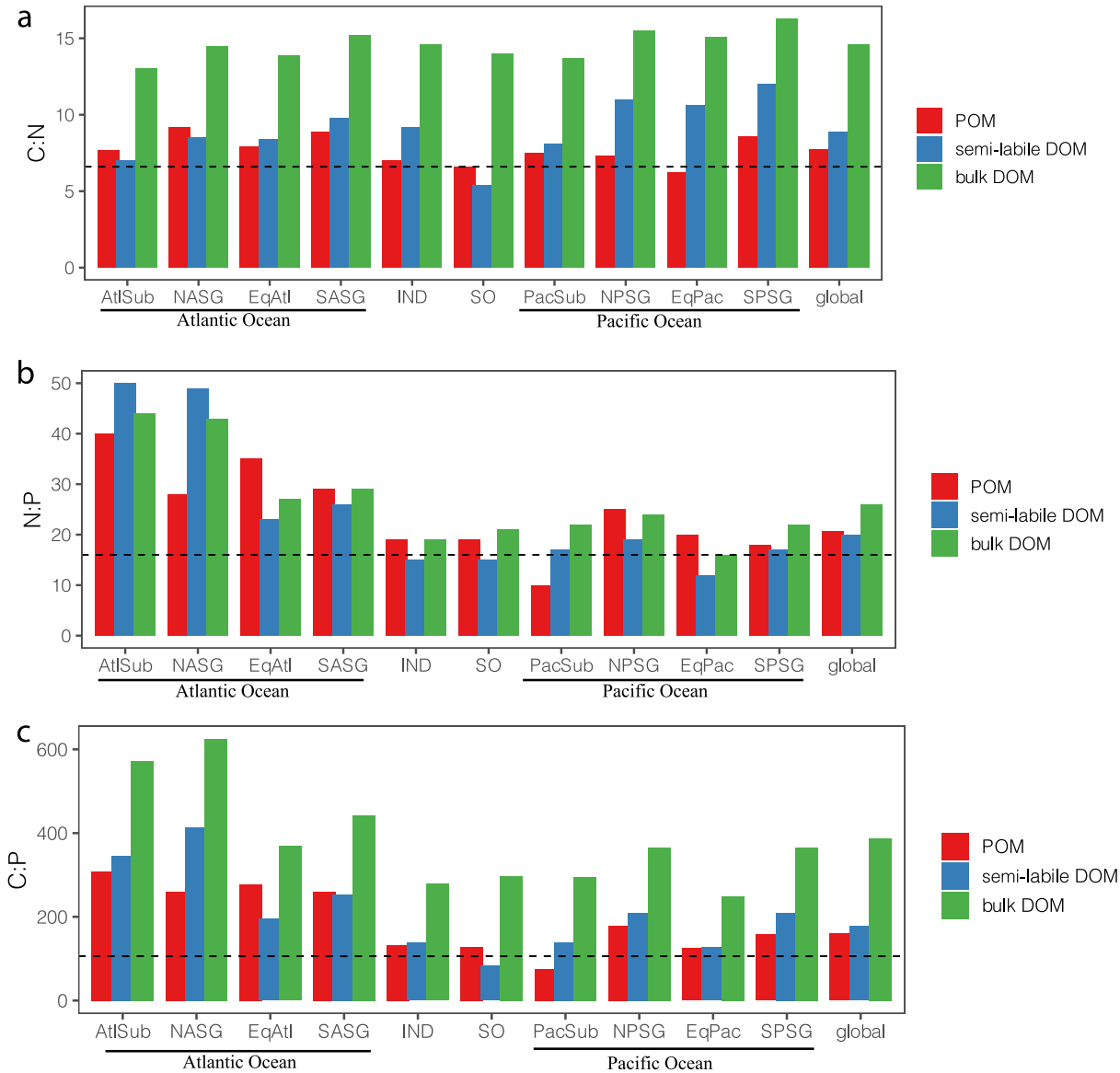

Figure 9. Comparison of surface ocean POM, semi-labile, and bulk DOM stoichiometry in different biogeochemical regions. The dashed line marks the canonical Redfield ratio (C:N:P = 106:16:1). C:N:P ratios in POM were calculated from global ocean POM concentration data sets (Martiny et al., 2014; Tanioka et al., 2022).

N and P from either inorganic or organic sources. Between 20°N to 40°N, consumption of DOP increases due to elevated PO_4^{3-} stress, with a resulting surface ocean DOM stoichiometric signature of extraordinarily elevated bulk and semi-labile DON:DOP (up to ~58:1) and DOC:DOP (up to ~745:1) concentration ratios (Figure 8). We suggest that other regions with relatively elevated bulk and semi-labile surface ocean DON:DOP (~27–30:1) and DOC:DOP (~400:1) concentration ratios, for example, the Western North and South Pacific and Western South Atlantic (Figures 1 and 5) (Tables 3, 4, 6, and 7) would continue to draw down surface ocean DOP concentrations if iron was more abundant.

4.4. Comparison Between Surface Ocean DOM and POM Stoichiometry

Finally, we compare our results in bulk and semi-labile surface ocean DOM stoichiometry with POM stoichiometry. Recent studies show that surface ocean POM C:N:P stoichiometry exhibits regional variability depending on nutrient stress and phytoplankton community composition (Galbraith & Martiny, 2015; Inomura et al., 2022; Lomas et al., 2021; Teng et al., 2014). Here, we use recent global POM concentration data sets

(Martiny et al., 2014; Tanioka et al., 2022) to calculate surface ocean POC:PON:POP stoichiometry in the same 10 biogeochemical regions (Table S4 in Supporting Information S1) and compare them with the bulk and semi-labile surface ocean DOC:DON:DOP stoichiometry (Figure 9). First, we find that bulk DOC:DON concentration ratios (C:N = 14.6:1) are higher than semi-labile DOC:DON and POC:PON concentration across all regions, with semi-labile DOC:DON and POC:PON concentration ratios more similar to each other, with a mean of 8.9:1 for semi-labile DOC:DON and 7.7:1 for POC:PON (Figure 9) (Table S4 in Supporting Information S1). These results suggest that semi-labile DOM and POM are produced with similar C:N ratios, with refractory DOM becoming more depleted in N either from preferential remineralization (Knapp, Casciotti, & Prokopenko, 2018; Knapp, McCabe, et al., 2018; Letscher & Moore, 2015), and/or potentially accumulating DOC from another source (McCarthy et al., 2004). We also note that semi-labile DOC:DON concentration ratios are systematically higher than POC:PON concentration ratios in the Pacific than in the Atlantic Ocean (Figure 9). We hypothesize that this results from preferential loss of surface ocean DON resulting from increased demand on the surface ocean DON pool due to dissimilatory inorganic N loss in the ODZs of the Eastern Pacific (Bif et al., 2022; Knapp, Casciotti, & Prokopenko, 2018), although additional field work would help evaluate this possibility.

Additionally, we find that semi-labile DOM, bulk DOM, and POM have similar N:P stoichiometry across different biogeochemical regions, with the exception of the NASG, where semi-labile and bulk DON:DOP stoichiometry (N:P = 43:1 for bulk DOM and N:P = 49:1 for semi-labile DOM) exceed PON:POP stoichiometry (N:P = 31:1) (Figure 9) (Table S4 in Supporting Information S1), suggesting that the NASG is a unique region with significant DOP consumption by phytoplankton. Typically, bulk DOC:DOP stoichiometry (global mean of 387:1) is higher than semi-labile DOC:DOP and POC:POP stoichiometry (global mean of 179:1 for semi-labile DOC:DOP and global mean of 160:1 for POC:POP), which are similar across the different biogeochemical regions (Figure 9). However, the NASG exhibits higher semi-labile DOC:DOP stoichiometry (C:P = 638:1) than POC:POP (C:P = 285:1), which we hypothesize results from autotrophic DOP consumption. We argue that the reduced P* and elevated dust deposition to the NASG sets it apart in the global ocean and increases demand on the surface ocean DOP pool as an alternative autotrophic nutrient source, consistent with previous studies on DOP cycling in the Sargasso Sea (Lomas et al., 2010; Mather et al., 2008; Orchard et al., 2010; Reynolds et al., 2014; Sohm & Capone, 2010; Van Mooy et al., 2009).

5. Conclusion

In this work we describe global patterns in surface ocean DOC:DON:DOP stoichiometry using updated global ocean DOC, DON and DOP concentration data sets (Hansell et al., 2021; Liang et al., 2022b). We find that bulk and semi-labile surface ocean DOC:DON stoichiometry exhibit the least spatial variability, consistent with prior work (Bif et al., 2022; Hansell & Carlson, 1998a, 2001), although the semi-labile DOC:DON stoichiometry is closer to the "Redfield" 6.6:1 C:N stoichiometry (on average ∼8.9:1) than bulk DOC:DON stoichiometry (on average ∼14.6:1). Additionally, significant differences in bulk and semi-labile surface ocean DON:DOP and DOC:DOP stoichiometry were observed within and among ocean basins, whether divided based on biogeochemical or geographical boundaries, and we argue that these trends are driven by the significant rates of water column denitrification occurring in the eastern tropical Pacific, and the high rates of atmospheric dust deposition to the tropical North Atlantic. Specifically, we find that bulk and semi-labile surface ocean DON:DOP and DOC:DOP stoichiometry increase from the East to West in the Pacific as a result of increasing demand on the DOP pool as surface waters transit westwards in the basin (Liang et al., 2022a). In the Atlantic, meridional increases in bulk and semi-labile surface ocean DON:DOP and DOC:DOP stoichiometry from the South to the North are coincident with regions of low iron stress and high PO_4^{3-} stress, and the lowest concentrations of surface ocean DOP observed globally. These observations illustrate the geochemical expression of subsurface (i.e., denitrification) and surface (i.e., atmospheric dust deposition) processes on surface ocean organic matter stoichiometry. We stress that these observations would not be possible without the considerable effort associated with basin-crossing cruises, including the CLIVAR, GO-SHIP, and GEOTRACES field campaigns, which provide unique synoptic insight into global marine biogeochemical processes.

Conflict of Interest

The authors declare no conflicts of interest relevant to this study.

Data Availability Statement

DOP concentration data were obtained from the DOPv2021 database (Knapp et al., 2022; Liang et al., 2022b). DOC and DON concentration data were derived from a compilation of DOM data obtained from global ocean observations from 1994 to 2021 (Hansell et al., 2021). Binned DOC, DON, and DOP concentration data on the OCIM2 grid are archived in Liang et al., 2023. All data are publicly available.

Acknowledgments
This research was funded by NSF-OCE–1829797 (ANK) and NSF-OCE-1829916 (RTL). We also acknowledge Tom Weber and Hairong Xu who kindly shared their model output of dust deposition rates. We gratefully acknowledge the scientists and crew who facilitated sample collection for the global DOC, DON, and DOP concentration databases.

References

Abell, J., Emerson, S., & Renaud, P. (2000). Distributions of TOP, TON and TOC in the North Pacific subtropical gyre: Implications for nutrient supply in the surface ocean and remineralization in the upper thermocline. *Journal of Marine Research*, *58*(2), 203–222. https://doi.org/10.1357/002224000321511142

Anderson, L. G., & Amon, R. M. W. (2015). Chapter 14—DOM in the Arctic Ocean. In D. A. Hansell, & C. A. Carlson (Eds.), *Biogeochemistry of Marine dissolved organic matter* (2nd ed., pp. 609–633). Academic Press. https://doi.org/10.1016/B978-0-12-405940-5.00014-5

Arrieta, J. M., Mayol, E., Hansman, R. L., Herndl, G. J., Dittmar, T., & Duarte, C. M. (2015). Dilution limits dissolved organic carbon utilization in the deep ocean. *Science*, *348*(6232), 331–333. https://doi.org/10.1126/science.1258955

Baker, A. R., Kelly, S. D., Biswas, K. F., Witt, M., & Jickells, T. D. (2003). Atmospheric deposition of nutrients to the Atlantic Ocean. *Geophysical Research Letters*, *30*(24), 2296. https://doi.org/10.1029/2003GL018518

Behrenfeld, M. J., & Falkowski, P. G. (1997). Photosynthetic rates derived from satellite-based chlorophyll concentration. *Limnology & Oceanography*, *42*(1), 1–20. https://doi.org/10.4319/lo.1997.42.1.0001

Behrenfeld, M. J., & Milligan, A. J. (2013). Photophysiological expressions of iron stress in phytoplankton. *Annual Review of Marine Science*, *5*(1), 217–246. https://doi.org/10.1146/annurev-marine-121211-172356

Behrenfeld, M. J., Westberry, T. K., Boss, E. S., O'Malley, R. T., Siegel, D. A., Wiggert, J. D., et al. (2009). Satellite-detected fluorescence reveals global physiology of ocean phytoplankton. *Biogeosciences*, *6*(5), 779–794. https://doi.org/10.5194/bg-6-779-2009

Benner, R., Louchouarn, P., & Amon, R. M. W. (2005). Terrigenous dissolved organic matter in the Arctic Ocean and its transport to surface and deep waters of the North Atlantic. *Global Biogeochemical Cycles*, *19*(2), GB2025. https://doi.org/10.1029/2004GB002398

Berges, J. A., & Mulholland, M. R. (2008). Chapter 32—Enzymes and nitrogen cycling. In D. G. Capone, D. A. Bronk, M. R. Mulholland, & E. J. Carpenter (Eds.), *Nitrogen in the marine environment* (2nd ed., pp. 1385–1444). Academic Press. https://doi.org/10.1016/B978-0-12-372522-6.00032-3

Bif, M. B., Bourbonnais, A., Hansell, D. A., Granger, J., Westbrook, H., & Altabet, M. A. (2022). Controls on surface distributions of dissolved organic carbon and nitrogen in the southeast Pacific Ocean. *Marine Chemistry*, *244*, 104136. https://doi.org/10.1016/j.marchem.2022.104136

Björkman, K. M., & Karl, D. M. (2003). Bioavailability of dissolved organic phosphorus in the euphotic zone at station ALOHA, North Pacific subtropical Gyre. *Limnology & Oceanography*, *48*(3), 1049–1057. https://doi.org/10.4319/lo.2003.48.3.1049

Bonnet, S., Guieu, C., Taillandier, V., Boulart, C., Bouruet-Aubertot, P., Gazeau, F., et al. (2023). Natural iron fertilization by shallow hydrothermal sources fuels diazotroph blooms in the ocean. *Science*, *380*(6647), 812–817. https://doi.org/10.1126/science.abq4654

Bronk, D. A., See, J. H., Bradley, P., & Killberg, L. (2007). DON as a source of bioavailable nitrogen for phytoplankton. *Biogeosciences*, *4*(3), 283–296. https://doi.org/10.5194/bg-4-283-2007

Browning, T. J., Bouman, H. A., & Moore, C. M. (2014). Satellite-detected fluorescence: Decoupling nonphotochemical quenching from iron stress signals in the South Atlantic and Southern Ocean. *Global Biogeochemical Cycles*, *28*(5), 510–524. https://doi.org/10.1002/2013GB004773

Carlson, C. A., Ducklow, H. W., & Michaels, A. F. (1994). Annual flux of dissolved organic carbon from the euphotic zone in the northwestern Sargasso Sea. *Nature*, *371*(6496), 405–408. https://doi.org/10.1038/371405a0

Carlson, C. A., & Hansell, D. A. (2015). Chapter 3—DOM sources, sinks, reactivity, and budgets. In D. A. Hansell & C. A. Carlson (Eds.), *Biogeochemistry of Marine dissolved organic matter* (2nd ed., pp. 65–126). Academic Press. https://doi.org/10.1016/B978-0-12-405940-5.00003-0

Carr, M.-E., Friedrichs, M. A. M., Schmeltz, M., Noguchi Aita, M., Antoine, D., Arrigo, K. R., et al. (2006). A comparison of global estimates of marine primary production from ocean color. *Deep Sea Research Part II: Topical Studies in Oceanography*, *53*(5), 741–770. https://doi.org/10.1016/j.dsr2.2006.01.028

Cavender-Bares, K. K., Karl, D. M., & Chisholm, S. W. (2001). Nutrient gradients in the western North Atlantic Ocean: Relationship to microbial community structure and comparison to patterns in the Pacific Ocean. *Deep Sea Research Part I: Oceanographic Research Papers*, *48*(11), 2373–2395. https://doi.org/10.1016/S0967-0637(01)00027-9

Chang, B. X., Devol, A. H., & Emerson, S. R. (2010). Denitrification and the nitrogen gas excess in the eastern tropical South Pacific oxygen deficient zone. *Deep Sea Research Part I: Oceanographic Research Papers*, *57*(9), 1092–1101. https://doi.org/10.1016/j.dsr.2010.05.009

Chang, B. X., Devol, A. H., & Emerson, S. R. (2012). Fixed nitrogen loss from the eastern tropical North Pacific and Arabian Sea oxygen deficient zones determined from measurements of N2:Ar. *Global Biogeochemical Cycles*, *26*(3), GB2025. https://doi.org/10.1029/2011GB004207

Cleveland, W. S. (1979). Robust locally weighted regression and smoothing scatterplots. *Journal of the American Statistical Association*, *74*(368), 829–836. https://doi.org/10.1080/01621459.1979.10481038

Connolly, C. T., Cardenas, M. B., Burkart, G. A., Spencer, R. G. M., & McClelland, J. W. (2020). Groundwater as a major source of dissolved organic matter to Arctic coastal waters. *Nature Communications*, *11*(1), 1479. https://doi.org/10.1038/s41467-020-15250-8

Dekaezemacker, J., Bonnet, S., Grosso, O., Moutin, T., Bressac, M., & Capone, D. g. (2013). Evidence of active dinitrogen fixation in surface waters of the eastern tropical South Pacific during El Niño and La Niña events and evaluation of its potential nutrient controls. *Global Biogeochemical Cycles*, *27*(3), 768–779. https://doi.org/10.1002/gbc.20063

Deutsch, C., Sarmiento, J. L., Sigman, D. M., Gruber, N., & Dunne, J. P. (2007). Spatial coupling of nitrogen inputs and losses in the ocean. *Nature*, *445*(7124), 163–167. https://doi.org/10.1038/nature05392

DeVries, T. (2022). The ocean carbon cycle. *Annual Review of Environment and Resources*, *47*(1), 317–341. https://doi.org/10.1146/annurev-environ-120920-111307

DeVries, T., & Deutsch, C. (2014). Large-scale variations in the stoichiometry of marine organic matter respiration. *Nature Geoscience*, *7*(12), 890–894. https://doi.org/10.1038/ngeo2300

DeVries, T., Deutsch, C., Primeau, F., Chang, B., & Devol, A. (2012). Global rates of water-column denitrification derived from nitrogen gas measurements. *Nature Geoscience*, *5*(8), 547–550. https://doi.org/10.1038/ngeo1515

DeVries, T., & Holzer, M. (2019). Radiocarbon and helium isotope constraints on deep ocean ventilation and mantle-^{3}He sources. *Journal of Geophysical Research: Oceans*, *124*(5), 3036–3057. https://doi.org/10.1029/2018JC014716

DeVries, T., & Weber, T. (2017). The export and fate of organic matter in the ocean: New constraints from combining satellite and oceanographic tracer observations. *Global Biogeochemical Cycles*, *31*(3), 535–555. https://doi.org/10.1002/2016GB005551

Dittmar, T., Lennartz, S. T., Buck-Wiese, H., Hansell, D. A., Santinelli, C., Vanni, C., et al. (2021). Enigmatic persistence of dissolved organic matter in the ocean. *Nature Reviews Earth & Environment*, *2*(8), 570–583. Article 8. https://doi.org/10.1038/s43017-021-00183-7

Druffel, E. R. M., Williams, P. M., Bauer, J. E., & Ertel, J. R. (1992). Cycling of dissolved and particulate organic matter in the open ocean. *Journal of Geophysical Research*, *97*(C10), 15639–15659. https://doi.org/10.1029/92JC01511

Duhamel, S., Diaz, J. M., Adams, J. C., Djaoudi, K., Steck, V., & Waggoner, E. M. (2021). Phosphorus as an integral component of global marine biogeochemistry. *Nature Geoscience*, *14*(6), 359–368. https://doi.org/10.1038/s41561-021-00755-8

Dyhrman, S. T., Chappell, P. D., Haley, S. T., Moffett, J. W., Orchard, E. D., Waterbury, J. B., & Webb, E. A. (2006). Phosphonate utilization by the globally important marine diazotroph *Trichodesmium*. *Nature*, *439*(7072), 68–71. https://doi.org/10.1038/nature04203

Emerson, S. (2014). Annual net community production and the biological carbon flux in the ocean. *Global Biogeochemical Cycles*, *28*(1), 14–28. https://doi.org/10.1002/2013GB004680

Fawcett, S. E., Lomas, M. W., Casey, J. R., Ward, B. B., & Sigman, D. M. (2011). Assimilation of upwelled nitrate by small eukaryotes in the Sargasso Sea. *Nature Geoscience*, *4*(10), 717–722. Article 10. https://doi.org/10.1038/ngeo1265

Follett, C. L., Repeta, D. J., Rothman, D. H., Xu, L., & Santinelli, C. (2014). Hidden cycle of dissolved organic carbon in the deep ocean. *Proceedings of the National Academy of Sciences of the United States of America*, *111*(47), 16706–16711. https://doi.org/10.1073/pnas.1407445111

Foreman, R. K., Björkman, K. M., Carlson, C. A., Opalk, K., & Karl, D. M. (2019). Improved ultraviolet photo-oxidation system yields estimates for deep-sea dissolved organic nitrogen and phosphorus. *Limnology and Oceanography: Methods*, *17*(4), 277–291. https://doi.org/10.1002/lom3.10312

Galbraith, E. D., & Martiny, A. C. (2015). A simple nutrient-dependence mechanism for predicting the stoichiometry of marine ecosystems. *Proceedings of the National Academy of Sciences of the United States of America*, *112*(27), 8199–8204. https://doi.org/10.1073/pnas.1423917112

Garcia, H. E., Locarnini, R. A., Boyer, T. P., Antonov, J. I., Baranova, O. K., Zweng, M. M., et al. (2013). World Ocean Atlas 2013, volume 4: Dissolved inorganic nutrients (phosphate, nitrate, silicate). In S. Levitus, & A. Mishonov (Eds.), *NOAA Atlas NESDIS* (Vol. 76, p. 25). Retrieved from https://repository.library.noaa.gov/view/noaa/14850

Gledhill, M., Hollister, A., Seidel, M., Zhu, K., Achterberg, E. P., Dittmar, T., & Koschinsky, A. (2022). Trace metal stoichiometry of dissolved organic matter in the Amazon plume. *Science Advances*, *8*(31), eabm2249. https://doi.org/10.1126/sciadv.abm2249

Gruber, N., Keeling, C. D., & Stocker, T. F. (1998). Carbon-13 constraints on the seasonal inorganic carbon budget at the BATS site in the northwestern Sargasso Sea. *Deep Sea Research Part I: Oceanographic Research Papers*, *45*(4), 673–717. https://doi.org/10.1016/S0967-0637(97)00098-8

Guieu, C., Bonnet, S., Petrenko, A., Menkes, C., Chavagnac, V., Desboeufs, K., et al. (2018). Iron from a submarine source impacts the productive layer of the Western Tropical South Pacific (WTSP). *Scientific Reports*, *8*(1), 9075. https://doi.org/10.1038/s41598-018-27407-z

Hain, M. P., Sigman, D. M., & Haug, G. H. (2014). The biological pump in the past. 2nd ed. (eds. In H. D. Holland & K. K. Turekian (Eds.),), *Treatise on geochemistry*, 485–517. Elsevier. https://doi.org/10.1016/B978-0-08-095975-7.00618-5

Hansell, D. A. (2013). Recalcitrant dissolved organic carbon fractions. *Annual Review of Marine Science*, *5*(1), 421–445. https://doi.org/10.1146/annurev-marine-120710-100757

Hansell, D. A., & Carlson, C. A. (1998a). Net community production of dissolved organic carbon. *Global Biogeochemical Cycles*, *12*(3), 443–453. https://doi.org/10.1029/98GB01928

Hansell, D. A., & Carlson, C. A. (1998b). Deep-ocean gradients in the concentration of dissolved organic carbon. *Nature*, *395*(6699), 263–266. https://doi.org/10.1038/26200

Hansell, D. A., & Carlson, C. A. (2001). Biogeochemistry of total organic carbon and nitrogen in the Sargasso Sea: Control by convective overturn. *Deep Sea Research Part II: Topical Studies in Oceanography*, *48*(8), 1649–1667. https://doi.org/10.1016/S0967-0645(00)00153-3

Hansell, D. A., Carlson, C. A., Amon, R. M. W., Álvarez-Salgado, X. A., Yamashita, Y., Romera-Castillo, C., & Bif, M. B. (2021). Compilation of dissolved organic matter (DOM) data obtained from global ocean observations from 1994 to 2021 (NCEI Accession 0227166) (version 1) [Dataset]. NOAA National Centers for Environmental Information. https://doi.org/10.25921/s4f4-ye35

Hansell, D. A., Carlson, C. A., Repeta, D. J., & Schlitzer, R. (2009). Dissolved organic matter in the ocean: A controversy stimulates new insights. *Oceanography*, *22*(4), 202–211. https://doi.org/10.5670/oceanog.2009.109

Hansell, D. A., Kadko, D., & Bates, N. R. (2004). Degradation of terrigenous dissolved organic carbon in the western Arctic Ocean. *Science*, *304*(5672), 858–861. https://doi.org/10.1126/science.1096175

Hashihama, F., Saito, H., Shiozaki, T., Ehama, M., Suwa, S., Sugiyama, T., et al. (2020). Biogeochemical controls of particulate phosphorus distribution across the oligotrophic subtropical Pacific Ocean. *Global Biogeochemical Cycles*, *34*(9), e2020GB006669. https://doi.org/10.1029/2020GB006669

Hopkinson, C. S., & Vallino, J. J. (2005). Efficient export of carbon to the deep ocean through dissolved organic matter. *Nature*, *433*(7022), 142–145. https://doi.org/10.1038/nature03191

Hopwood, M. J., Carroll, D., Browning, T. J., Meire, L., Mortensen, J., Krisch, S., & Achterberg, E. P. (2018). Non-linear response of summertime marine productivity to increased meltwater discharge around Greenland. *Nature Communications*, *9*(1), 3256. https://doi.org/10.1038/s41467-018-05488-8

Inomura, K., Deutsch, C., Jahn, O., Dutkiewicz, S., & Follows, M. J. (2022). Global patterns in marine organic matter stoichiometry driven by phytoplankton ecophysiology. *Nature Geoscience*, *15*(12), 1034–1040. https://doi.org/10.1038/s41561-022-01066-2

Jickells, T., & Moore, C. M. (2015). The importance of atmospheric deposition for ocean productivity. *Annual Review of Ecology, Evolution, and Systematics*, *46*(1), 481–501. https://doi.org/10.1146/annurev-ecolsys-112414-054118

John, S. G., Liang, H., Weber, T., DeVries, T., Primeau, F., Moore, K., et al. (2020). AWESOME OCIM: A simple, flexible, and powerful tool for modeling elemental cycling in the oceans. *Chemical Geology*, *533*, 119403. https://doi.org/10.1016/j.chemgeo.2019.119403

Johnson, K. S., Riser, S. C., & Karl, D. M. (2010). Nitrate supply from deep to near-surface waters of the North Pacific subtropical gyre. *Nature*, *465*(7301), 1062–1065. https://doi.org/10.1038/nature09170

Kadko, D., & Johns, W. (2011). Inferring upwelling rates in the equatorial Atlantic using ^{7}Be measurements in the upper ocean. *Deep Sea Research Part I: Oceanographic Research Papers*, *58*(6), 647–657. https://doi.org/10.1016/j.dsr.2011.03.004

Kathuria, S., & Martiny, A. C. (2011). Prevalence of a calcium-based alkaline phosphatase associated with the marine cyanobacterium *Prochlorococcus* and other ocean bacteria. *Environmental Microbiology*, *13*(1), 74–83. https://doi.org/10.1111/j.1462-2920.2010.02310.x

Keeling, C. D., Brix, H., & Gruber, N. (2004). Seasonal and long-term dynamics of the upper ocean carbon cycle at Station ALOHA near Hawaii. *Global Biogeochemical Cycles*, *18*(4), GB4006. https://doi.org/10.1029/2004GB002227

Knapp, A. N., Casciotti, K. L., Berelson, W. M., Prokopenko, M. G., & Capone, D. G. (2016). Low rates of nitrogen fixation in eastern tropical South Pacific surface waters. *Proceedings of the National Academy of Sciences of the United States of America*, *113*(16), 4398–4403. https://doi.org/10.1073/pnas.1515641113

Knapp, A. N., Casciotti, K. L., & Prokopenko, M. G. (2018). Dissolved organic nitrogen production and consumption in eastern tropical South Pacific surface waters. *Global Biogeochemical Cycles*, *32*(5), 769–783. https://doi.org/10.1029/2017GB005875

Knapp, A. N., Hastings, M. G., Sigman, D. M., Lipschultz, F., & Galloway, J. N. (2010). The flux and isotopic composition of reduced and total nitrogen in Bermuda rain. *Marine Chemistry*, *120*(1), 83–89. https://doi.org/10.1016/j.marchem.2008.08.007

Knapp, A. N., Liang, Z., & Letscher, R. T. (2022). DOP concentration observations from the global ocean between 1990 and 2021 (DOP N2 fixation and export production project) (version 3) [Dataset]. Biological and Chemical Oceanography Data Management Office (BCO-DMO). https://doi.org/10.26008/1912/bco-dmo.855139.3

Knapp, A. N., McCabe, K. M., Grosso, O., Leblond, N., Moutin, T., & Bonnet, S. (2018). Distribution and rates of nitrogen fixation in the western tropical South Pacific Ocean constrained by nitrogen isotope budgets. *Biogeosciences*, *15*(9), 2619–2628. https://doi.org/10.5194/bg-15-2619-2018

Knapp, A. N., Sigman, D. M., & Lipschultz, F. (2005). N isotopic composition of dissolved organic nitrogen and nitrate at the Bermuda Atlantic Time-series Study site. *Global Biogeochemical Cycles*, *19*(1). https://doi.org/10.1029/2004GB002320

Knapp, A. N., Sigman, D. M., Lipschultz, F., Kustka, A. B., & Capone, D. G. (2011). Interbasin isotopic correspondence between upper-ocean bulk DON and subsurface nitrate and its implications for marine nitrogen cycling. *Global Biogeochemical Cycles*, *25*(4), GB4004. https://doi.org/10.1029/2010GB003878

Knapp, A. N., Thomas, R. K., Stukel, M. R., Kelly, T. B., Landry, M. R., Selph, K. E., et al. (2021). Constraining the sources of nitrogen fueling export production in the Gulf of Mexico using nitrogen isotope budgets. *Journal of Plankton Research*, *44*(5), 692–710. https://doi.org/10.1093/plankt/fbab049

Lang, S. Q., Butterfield, D. A., Lilley, M. D., Paul Johnson, H., & Hedges, J. I. (2006). Dissolved organic carbon in ridge-axis and ridge-flank hydrothermal systems. *Geochimica et Cosmochimica Acta*, *70*(15), 3830–3842. https://doi.org/10.1016/j.gca.2006.04.031

Lee, J. A., Garcia, C. A., Larkin, A. A., Carter, B. R., & Martiny, A. C. (2021). Linking a latitudinal gradient in ocean hydrography and elemental stoichiometry in the eastern Pacific Ocean. *Global Biogeochemical Cycles*, *35*(5), e2020GB006622. https://doi.org/10.1029/2020GB006622

Letscher, R., Primeau, F., & Moore, J. (2016). Nutrient budgets in the subtropical ocean gyres dominated by lateral transport. *Nature Geoscience*, *9*(11), 815–819. https://doi.org/10.1038/NGEO2812

Letscher, R. T., Hansell, D. A., Carlson, C. A., Lumpkin, R., & Knapp, A. N. (2013). Dissolved organic nitrogen in the global surface ocean: Distribution and fate. *Global Biogeochemical Cycles*, *27*(1), 141–153. https://doi.org/10.1029/2012GB004449

Letscher, R. T., & Moore, J. K. (2015). Preferential remineralization of dissolved organic phosphorus and non-Redfield DOM dynamics in the global ocean: Impacts on marine productivity, nitrogen fixation, and carbon export. *Global Biogeochemical Cycles*, *29*(3), 325–340. https://doi.org/10.1002/2014GB004904

Letscher, R. T., Moore, J. K., Teng, Y.-C., & Primeau, F. (2015). Variable C: N: P stoichiometry of dissolved organic matter cycling in the community Earth system model. *Biogeosciences*, *12*(1), 209–221. https://doi.org/10.5194/bg-12-209-2015

Letscher, R. T., Wang, W.-L., Liang, Z., & Knapp, A. N. (2022). Regionally variable contribution of dissolved organic phosphorus to marine annual net community production. *Global Biogeochemical Cycles*, *36*(12), e2022GB007354. https://doi.org/10.1029/2022GB007354

Li, T., Guo, C., Zhang, Y., Wang, C., Lin, X., & Lin, S. (2018). Identification and expression analysis of an atypical alkaline phosphatase in *Emiliania huxleyi*. *Frontiers in Microbiology*, *9*. https://doi.org/10.3389/fmicb.2018.02156

Liang, Z., Letscher, R. T., & Knapp, A. N. (2022a). Dissolved organic phosphorus concentrations in the surface ocean controlled by both phosphate and iron stress. *Nature Geoscience*, *15*(8), 651–657. https://doi.org/10.1038/s41561-022-00988-1

Liang, Z., Letscher, R. T., & Knapp, A. N. (2023). Binned dissolved organic carbon (DOC), dissolved organic nitrogen (DON), and dissolved organic phosphorus (DOP) concentration observations in the ocean (version 1) [Dataset]. Zenodo. https://doi.org/10.5281/zenodo.8432153

Liang, Z., McCabe, K., Fawcett, S. E., Forrer, H. J., Hashihama, F., Jeandel, C., et al. (2022b). A global ocean dissolved organic phosphorus concentration database (DOPv2021). *Scientific Data*, *9*(1), 772. https://doi.org/10.1038/s41597-022-01873-7

Lomas, M. W., Baer, S. E., Mouginot, C., Terpis, K. X., Lomas, D. A., Altabet, M. A., & Martiny, A. C. (2021). Varying influence of phytoplankton biodiversity and stoichiometric plasticity on bulk particulate stoichiometry across ocean basins. *Communications Earth & Environment*, *2*(1), 143. https://doi.org/10.1038/s43247-021-00212-9

Lomas, M. W., Burke, A. L., Lomas, D. A., Bell, D. W., Shen, C., Dyhrman, S. T., & Ammerman, J. W. (2010). Sargasso Sea phosphorus biogeochemistry: An important role for dissolved organic phosphorus (DOP). *Biogeosciences*, *7*(2), 695–710. https://doi.org/10.5194/bg-7-695-2010

Lønborg, C., Álvarez–Salgado, X. A., Letscher, R. T., & Hansell, D. A. (2018). Large stimulation of recalcitrant dissolved organic carbon degradation by increasing ocean temperatures. *Frontiers in Marine Science*, *4*. https://doi.org/10.3389/fmars.2017.00436

Mahadevan, A. (2016). The impact of submesoscale physics on primary productivity of plankton. *Annual Review of Marine Science*, *8*(1), 161–184. https://doi.org/10.1146/annurev-marine-010814-015912

Mahowald, N. M., Baker, A. R., Bergametti, G., Brooks, N., Duce, R. A., Jickells, T. D., et al. (2005). Atmospheric global dust cycle and iron inputs to the ocean. *Global Biogeochemical Cycles*, *19*(4), GB4025. https://doi.org/10.1029/2004GB002402

Martin, P., Dyhrman, S. T., Lomas, M. W., Poulton, N. J., & Mooy, B. A. S. V. (2014). Accumulation and enhanced cycling of polyphosphate by Sargasso Sea plankton in response to low phosphorus. *Proceedings of the National Academy of Sciences*, *111*(22), 8089–8094. https://doi.org/10.1073/pnas.1321719111

Martiny, A. C., Pham, C. T. A., Primeau, F. W., Vrugt, J. A., Moore, J. K., Levin, S. A., & Lomas, M. W. (2013). Strong latitudinal patterns in the elemental ratios of marine plankton and organic matter. *Nature Geoscience*, *6*(4), 279–283. https://doi.org/10.1038/ngeo1757

Martiny, A. C., Vrugt, J. A., & Lomas, M. W. (2014). Concentrations and ratios of particulate organic carbon, nitrogen, and phosphorus in the global ocean. *Scientific Data*, *1*(1), 140048. https://doi.org/10.1038/sdata.2014.48

Mather, R. L., Reynolds, S. E., Wolff, G. A., Williams, R. G., Torres-Valdes, S., Woodward, E. M. S., et al. (2008). Phosphorus cycling in the North and South Atlantic Ocean subtropical gyres. *Nature Geoscience*, *1*(7), 439–443. https://doi.org/10.1038/ngeo232

McCarthy, M. D., Benner, R., Lee, C., Hedges, J. I., & Fogel, M. L. (2004). Amino acid carbon isotopic fractionation patterns in oceanic dissolved organic matter: An unaltered photoautotrophic source for dissolved organic nitrogen in the ocean? *Marine Chemistry*, *92*(1), 123–134. https://doi.org/10.1016/j.marchem.2004.06.021

Medeiros, P. M., Seidel, M., Ward, N. D., Carpenter, E. J., Gomes, H. R., Niggemann, J., et al. (2015). Fate of the Amazon River dissolved organic matter in the tropical Atlantic Ocean. *Global Biogeochemical Cycles*, *29*(5), 677–690. https://doi.org/10.1002/2015GB005115

Moore, C. M., Mills, M. M., Arrigo, K. R., Berman-Frank, I., Bopp, L., Boyd, P. W., et al. (2013). Processes and patterns of oceanic nutrient limitation. *Nature Geoscience*, *6*(9), 701–710. https://doi.org/10.1038/ngeo1765

Mopper, K., Kieber, D. J., & Stubbins, A. (2015). In D. A. Hansell & C. A. Carlson (Eds.), *Chapter 8—Marine photochemistry of organic matter: Processes and IMPACTS*, *Biogeochemistry of marine dissolved organic matter* (2nd ed., pp. 389–450). Academic Press. https://doi.org/10.1016/B978-0-12-405940-5.00008-X

Orchard, E. D., Ammerman, J. W., Lomas, M. W., & Dyhrman, S. T. (2010). Dissolved inorganic and organic phosphorus uptake in *Trichodesmium* and the microbial community: The importance of phosphorus ester in the Sargasso Sea. *Limnology & Oceanography*, *55*(3), 1390–1399. https://doi.org/10.4319/lo.2010.55.3.1390

Paulmier, A., & Ruiz-Pino, D. (2009). Oxygen minimum zones (OMZs) in the modern ocean. *Progress in Oceanography*, *80*(3), 113–128. https://doi.org/10.1016/j.pocean.2008.08.001

Raymond, P. A., & Spencer, R. G. M. (2015). In D. A. Hansell & C. A. Carlson (Eds.), *Chapter 11—Riverine DOM. Biogeochemistry of Marine dissolved organic matter* (2nd ed., pp. 509–533). Academic Press. https://doi.org/10.1016/B978-0-12-405940-5.00011-X

Redfield, A. C. (1934). On the proportions of organic derivations in seawater and their relation to the composition of plankton. *James Johnstone memorial*, 176–192.

Reynolds, S., Mahaffey, C., Roussenov, V., & Williams, R. G. (2014). Evidence for production and lateral transport of dissolved organic phosphorus in the eastern subtropical North Atlantic. *Global Biogeochemical Cycles*, *28*(8), 805–824. https://doi.org/10.1002/2013GB004801

Romera-Castillo, C., Letscher, R. T., & Hansell, D. A. (2016). New nutrients exert fundamental control on dissolved organic carbon accumulation in the surface Atlantic Ocean. *Proceedings of the National Academy of Sciences of the United States of America*, *113*(38), 10497–10502. https://doi.org/10.1073/pnas.1605344113

Roshan, S., & DeVries, T. (2017). Efficient dissolved organic carbon production and export in the oligotrophic ocean. *Nature Communications*, *8*(1), 2036. https://doi.org/10.1038/s41467-017-02227-3

Siegel, D. A., DeVries, T., Cetinić, I., & Bisson, K. M. (2023). Quantifying the ocean's biological pump and its carbon cycle impacts on global scales. *Annual Review of Marine Science*, *15*(1), 329–356. https://doi.org/10.1146/annurev-marine-040722-115226

Simon, M., & Azam, F. (1989). Protein content and protein synthesis rates of planktonic marine bacteria. *Marine Ecology Progress Series*, *51*(3), 201–213. https://doi.org/10.3354/meps051201

Singh, A., Baer, S. E., Riebesell, U., Martiny, A. C., & Lomas, M. W. (2015). C: N: P stoichiometry at the Bermuda Atlantic time-series study station in the North Atlantic Ocean. *Biogeosciences*, *12*(21), 6389–6403. https://doi.org/10.5194/bg-12-6389-2015

Sipler, R. E., & Bronk, D. A. (2015). Chapter 4—Dynamics of dissolved organic nitrogen. 2nd edn. In D. A. Hansell & C. A. Carlson (Eds.), *Biogeochemistry of marine dissolved organic matter* (2nd ed., pp. 127–232). Academic Press. https://doi.org/10.1016/B978-0-12-405940-5.00004-2

Sohm, J. A., & Capone, D. G. (2010). Zonal differences in phosphorus pools, turnover and deficiency across the tropical North Atlantic Ocean. *Global Biogeochemical Cycles*, *24*(2), GB2008. https://doi.org/10.1029/2008GB003414

Stanley, R. H. R., Jenkins, W. J., Doney, S. C., & Lott, D. E., III. (2015). The ^{3}He flux gauge in the Sargasso Sea: A determination of physical nutrient fluxes to the euphotic zone at the Bermuda Atlantic time-series site. *Biogeosciences*, *12*(17), 5199–5210. https://doi.org/10.5194/bg-12-5199-2015

Tanioka, T., Larkin, A. A., Moreno, A. R., Brock, M. L., Fagan, A. J., Garcia, C. A., et al. (2022). Global ocean particulate organic phosphorus, carbon, oxygen for respiration, and Nitrogen (GO-POPCORN). *Scientific Data*, *9*(1), 688. https://doi.org/10.1038/s41597-022-01809-1

Teng, Y.-C., Primeau, F. W., Moore, J. K., Lomas, M. W., & Martiny, A. C. (2014). Global-scale variations of the ratios of carbon to phosphorus in exported marine organic matter. *Nature Geoscience*, *7*(12), 895–898. https://doi.org/10.1038/ngeo2303

Torres-Valdés, S., Roussenov, V. M., Sanders, R., Reynolds, S., Pan, X., Mather, R., et al. (2009). Distribution of dissolved organic nutrients and their effect on export production over the Atlantic Ocean. *Global Biogeochemical Cycles*, *23*(4), GB4019. https://doi.org/10.1029/2008GB003389

Trujillo-Ortiz, A., & Hernandez-Walls, R. (2021). Gmregress: Geometric mean regression (reduced major axis regression. A MATLAB file. Retrieved from http://www.mathworks.com/matlabcentral/fileexchange/27918-gmregress

Ustick, L. J., Larkin, A. A., Garcia, C. A., Garcia, N. S., Brock, M. L., Lee, J. A., et al. (2021). Metagenomic analysis reveals global-scale patterns of ocean nutrient limitation. *Science*, *372*(6539), 287–291. https://doi.org/10.1126/science.abe6301

Van Mooy, B. A. S., Fredricks, H. F., Pedler, B. E., Dyhrman, S. T., Karl, D. M., Koblížek, M., et al. (2009). Phytoplankton in the ocean use non-phosphorus lipids in response to phosphorus scarcity. *Nature*, *458*(7234), 69–72. https://doi.org/10.1038/nature07659

Villareal, T. A., Altabet, M. A., & Culver-Rymsza, K. (1993). Nitrogen transport by vertically migrating diatom mats in the North Pacific Ocean. *Nature*, *363*(6431), 709–712. https://doi.org/10.1038/363709a0

Wang, W.-L., Moore, J. K., Martiny, A. C., & Primeau, F. W. (2019). Convergent estimates of marine nitrogen fixation. *Nature*, *566*(7743), 205–211. https://doi.org/10.1038/s41586-019-0911-2

Ward, B. B., Devol, A. H., Rich, J. J., Chang, B. X., Bulow, S. E., Naik, H., et al. (2009). Denitrification as the dominant nitrogen loss process in the Arabian Sea. *Nature*, *461*(7260), 78–81. https://doi.org/10.1038/nature08276

Westberry, T., Behrenfeld, M. J., Siegel, D. A., & Boss, E. (2008). Carbon-based primary productivity modeling with vertically resolved photoacclimation. *Global Biogeochemical Cycles*, *22*(2), GB2024. https://doi.org/10.1029/2007GB003078

Wirtz, K., Smith, S. L., Mathis, M., & Taucher, J. (2022). Vertically migrating phytoplankton fuel high oceanic primary production. *Nature Climate Change*, *12*(8), 750–756. https://doi.org/10.1038/s41558-022-01430-5

Wu, J., Sunda, W., Boyle, E. A., & Karl, D. M. (2000). Phosphate depletion in the western north Atlantic Ocean. *Science*, *289*(5480), 759–762. https://doi.org/10.1126/science.289.5480.759

Xu, H., & Weber, T. (2021). Ocean dust deposition rates constrained in a data-assimilation model of the marine aluminum cycle. *Global Biogeochemical Cycles*, *35*(9), e2021GB007049. https://doi.org/10.1029/2021GB007049

Zakem, E. J., Cael, B. B., & Levine, N. M. (2021). A unified theory for organic matter accumulation. *Proceedings of the National Academy of Sciences of the United States of America*, *118*(6), e2016896118. https://doi.org/10.1073/pnas.2016896118

Zehr, J. P., & Ward, B. B. (2002). Nitrogen cycling in the ocean: New perspectives on processes and paradigms. *Applied and Environmental Microbiology*, *68*(3), 1015–1024. https://doi.org/10.1128/AEM.68.3.1015-1024.2002

Zhang, R., Wang, X. T., Ren, H., Huang, J., Chen, M., & Sigman, D. M. (2020). Dissolved organic nitrogen cycling in the South China Sea from an isotopic perspective. *Global Biogeochemical Cycles*, *34*(12), e2020GB006551. https://doi.org/10.1029/2020GB006551

Zhang, X., Ward, B. B., & Sigman, D. M. (2020). Global nitrogen cycle: Critical enzymes, organisms, and processes for nitrogen budgets and dynamics. *Chemical Reviews*, *120*(12), 5308–5351. https://doi.org/10.1021/acs.chemrev.9b00613

Zhang, Y., Mahowald, N., Scanza, R. A., Journet, E., Desboeufs, K., Albani, S., et al. (2015). Modeling the global emission, transport and deposition of trace elements associated with mineral dust. *Biogeosciences*, *12*(19), 5771–5792. https://doi.org/10.5194/bg-12-5771-2015